

NUMERICAL INVESTIGATION OF ELECTROMAGNETIC
SCATTERING FROM THE OCEAN SURFACE AT
EXTREME GRAZING ANGLES

By

RUIMIN CHEN

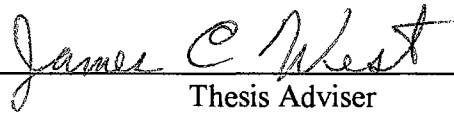
Bachelor of Science
Chongqing University
Chongqing, China
1982

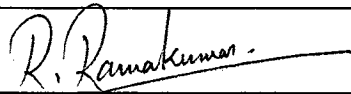
Master of Science
Chongqing University
Chongqing, China
1985

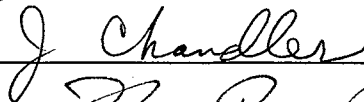
Submitted to the Faculty of the
Graduate College of the
Oklahoma State University
in Partial Fulfillment of
the Requirements for
the Degree of
DOCTOR OF PHILOSOPHY
May, 1994

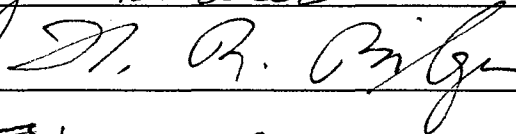
NUMERICAL INVESTIGATION OF ELECTROMAGNETIC
SCATTERING FROM THE OCEAN SURFACE AT
EXTREME GRAZING ANGLES

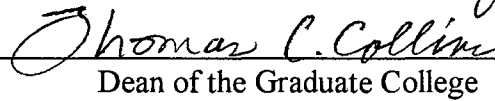
Thesis Approved:


Thesis Adviser








Dean of the Graduate College

PREFACE

The investigation of radar scattering from the ocean surface at large angles of incidence (small grazing angles) is of interest for scientific and military applications. Many approximate theories exist to describe scattering from the ocean surface, but their validity at small grazing angles is unknown. Traditional numerical techniques for surface scattering calculations cannot be directly applied under these conditions. In this work the moment method is extended to model rough surface scattering at very large angles. The modeled surface is treated as periodic, thereby eliminating nonphysical edge diffraction effects. A set of universal summations that are common to all moment method matrix elements are derived to efficiently evaluate the infinite summations that appear in integral equations describing scattering from periodic surfaces. Computational efforts to apply the technique to model reflection from an infinite flat plate and scattering from simple slightly rough surfaces confirm that the edge effects, including those at great incident angles, are reduced to acceptable levels.

The extended moment method has been applied to evaluate the scattering from random rough surfaces whose power spectral densities are defined by both Gaussian and power law functions. The treatment of Gaussian surfaces confirms that the technique can be used to accurately calculate the scattering from random rough surfaces at incidence angles up to at least 89° . At horizontal polarization, comparison of the numerically calculated scattering with the predictions of existing approximate theories shows that these theories can be applied at large incidence angles under the same surface conditions for which they were already known to be valid at moderate incidence angles. At vertical polarization, the approximate theories fail at extremely large incidence angles. The threshold at which the theories fail depends strongly on the surface roughness characteristics.

ACKNOWLEDGMENTS

I wish to express my sincere gratitude to the individuals who assisted me in this research work and during my coursework at Oklahoma State University. In particular, I would like to express my appreciation to my adviser, Dr. James C. West, for his encouragement, guidance, inspiration, and invaluable assistance over the last four years. He provided many helpful numerical routines and materials for this work. I also wish to thank the other committee members, Prof. H. R. Bilger, Prof. J. Chandler, Prof. R. G. Ramakumar and Dr. R. Zaroni, for the many helpful discussions, suggestions and support throughout the preparation of this work.

This work was supported in part through funding by the Office of Naval Research under contract N00014-92-5-1206.

This dissertation is dedicated to my parents, Deshen Chen and Xilan Duan, for their understanding and support during the long and difficult times that made this work possible. It is also dedicated to my wife Ping Huang and our son Zhe Chen for their loving encouragement, understanding, and other assistance over the many years during which this work was performed.

TABLE OF CONTENTS

| Chapter | Page |
|--|------|
| I. INTRODUCTION | 1 |
| II. INTEGRAL EQUATIONS AND THE MOMENT METHOD | 4 |
| Introduction | 4 |
| Electric Field Integral Equation (EFIE)..... | 4 |
| Magnetic Field Integral Equation (MFIE)..... | 7 |
| Moment Method with Point Matching | 9 |
| Basis Functions | 10 |
| Choice of Basis and Weighting Functions..... | 13 |
| III. APPLICATION OF MOMENT METHOD TO PERIODIC SURFACES..... | 15 |
| Introduction | 15 |
| Model of Integral Equations for Periodic Structure | 15 |
| EFIE for TM Polarization | 15 |
| MFIE for TM Polarization | 17 |
| MFIE for TE Polarization | 18 |
| Moment Method with Periodic Surface | 19 |
| EFIE PS Model for TM Polarization | 19 |
| MFIE PS Model for TM Polarization..... | 20 |
| MFIE PS Model for TE Polarization..... | 20 |
| Universal Summations | 21 |
| EFIE TM Polarization | 23 |
| MFIE TM Polarization | 26 |
| MFIE TE Polarization | 28 |
| IV. ERRORS AND COMPUTATIONAL-TIME ANALYSIS FOR PERIODIC-SURFACE MODEL..... | 29 |
| Introduction | 29 |
| Error Analysis for EFIE Periodic Surface Model | 29 |
| Truncation Errors... .. | 30 |
| Discretization Errors | 32 |

| | |
|--|----|
| Error with Period Length | 33 |
| Error of Using Approximate Hankel Functions | 34 |
| Error Analysis for MFIE Periodic Surface Model | 35 |
| Computational-Time Analysis for PS Model | 38 |
| V. SCATTERING CALCULATIONS FROM SIMPLE SURFACES | 40 |
| Introduction | 40 |
| Calculation of Scattering Coefficient | 40 |
| TM (Horizontal) Polarization | 40 |
| TE (Vertical) Polarization | 42 |
| Scattering from Simple Surfaces at Horizontal Polarization | 43 |
| Scattering from an Infinite Plane..... | 43 |
| Scattering from a Simple Sinusoidal Surface | 44 |
| Scattering from Simple Surface at Vertical Polarization..... | 47 |
| VI. ROUGH-SURFACE SCATTERING CALCULATIONS | 48 |
| Introduction | 48 |
| Traditional Scattering Models and techniques | 48 |
| The Kirchhoff Scattering Model (KS) | 48 |
| The Small Perturbation Model (SPM) | 50 |
| Moment Method with Illumination Weighting Function | 51 |
| Scattering Calculations..... | 52 |
| Generation of random surface..... | 53 |
| Scattering from Gaussian Surfaces | 54 |
| Results..... | 57 |
| Discussions..... | 62 |
| Scattering from Power-Law Surfaces | 66 |
| Results..... | 69 |
| Discussions..... | 73 |
| VII. SUMMARY AND CONCLUSIONS | 75 |
| REFERENCES | 78 |
| VITA..... | 83 |

LIST OF TABLES

| Table | Page |
|---|------|
| 1. Surface lengths (units) used in moment method computations for different incident radar wave lengths and various incident angles | 56 |
| 2. Parameters used in power-law surface scattering calculations..... | 68 |
| 3. Surface lengths used in PS model computation in power-law surface scattering calculations for different K_0 | 68 |

LIST OF FIGURES

| Figure | Page |
|--|------|
| 1. Geometry for two-dimensional scattering problems, TM polarization case | 6 |
| 2. Geometry for two-dimensional scattering problems, TE polarization case | 9 |
| 3. A set of pulse basis functions used for representing an arbitrary function $f(x)$ | 12 |
| 4. General problem of scattering from a periodic surface | 16 |
| 5. Geometry for an infinite plane scattering problem, TM polarization case | 22 |
| 6. Current distributions for PS model with various periodic sections M , scattering from an infinite flat plane, TM polarization, $\theta_i = 88^\circ$ | 22 |
| 7. Comparison of RMS relative errors of the calculated current on an infinite flat plane using EFIE PS model with various periodic sections (M) vs. incident angle, TM polarization case..... | 31 |
| 8. Discretization errors of the calculated current on an infinite flat plane using EFIE PS model for various basis functions per wavelength vs. incident angle, TM polarization | 32 |
| 9. RMS relative errors of the calculated current on an infinite flat plane using EFIE PS model Vs. various period length L , sampling rate $10/\lambda$, TM polarization..... | 33 |
| 10. Calculated currents using EFIE and MFIE PS models for a sinusoidal surface, $K=k$, $h=0.1\lambda$, $\theta_i = 88$ degree, TM polarization case..... | 36 |
| 11. Comparison of RMS relative errors of the calculated current using MFIE PS model for various periodic sections vs. incident angle, sinusoidal surface, $K=k$, $h=0.1\lambda$, TM polarization case..... | 37 |
| 12. Comparison of Computational time for the exact summation and the universal summation with various M . $N_m=100$ moment segments | 38 |
| 13. Backscattering coefficient calculated using the EFIE PS model for an infinite plane with various M | 44 |
| 14. Backscattering coefficient calculated using the EFIE PS model for an | |

| | |
|--|----|
| infinite sinusoidal surface ($h=0.1\lambda$, $K=1.1k$) for various values of M | 45 |
| 15. Backscattering coefficient calculated using the MFIE and EFIE PS model for an infinite sinusoidal surface ($h=0.1\lambda$, $K=1.1k$) for various value of M | 46 |
| 16. Backscattering coefficient (vertical polarization) for the PS model with various M from an infinite sinusoidal surface ($L=10$ unit, $h=0.1\lambda$, $K=1.1k$, $p_0=2$)..... | 47 |
| 17. A typical Gaussian surface and its autocorrelation function. $l=4$ units, $\sigma=1$ unit..... | 55 |
| 18. Backscattering coefficient of Gaussian surface, $\sigma=1.432$ units, horizontal polarization..... | 57 |
| 19. Backscattering coefficient of Gaussian surface, $\sigma=1.432$ units, vertical polarization | 60 |
| 20. Backscattering coefficient of Gaussian surface, $\sigma=0.7163$ units, horizontal polarization..... | 62 |
| 21. Backscattering coefficient of Gaussian surface, $\sigma=0.7163$ units, vertical polarization..... | 64 |
| 22. A typical power-law spectrum periodic surface and its autocorrelation function. $K_0=3$ | 67 |
| 23. Backscattering coefficient of power-law surface (K^{-3}) at horizontal polarization..... | 69 |
| 24. Backscattering coefficient of power-law surface (K^{-3}) at vertical polarization..... | 72 |

NOMENCLATURE

| | |
|---------------|--|
| EFIE | electrical field integral equation |
| E^i | incident electric field |
| E^s | scattered electric field |
| E_t | tangential component of electric field on surface |
| $G()$ | Green function in three dimensional form |
| $H()$ | Hankel function |
| H^i | incident magnetic field |
| H^s | scattering magnetic field |
| J_s | current on surface |
| J_0 | current on the reference periodic surface |
| k | radar wave number |
| K | surface wave number |
| KS | Kirchhoff scattering model |
| L | periodic surface length |
| M | upper limit for universal summations |
| MFIE | magnetic field integral equation |
| MMTW | moment method with tapered illumination weighting function |
| N_m | number of moment segments |
| N_s | number of surfaces averaged for scattering calculation |
| \hat{n} | unit vector normal to surface |
| p_0 | upper limit of summation terms using exact evaluation of the Hankel function |
| PS | periodic-surface moment method model |
| \mathbf{r} | position vector of observation point |
| \mathbf{r}' | position vector of source point |
| R | distance from observation point to source point |

| | |
|------------|--|
| SPM | small perturbation scattering model |
| $[V_m]$ | moment-method source vector |
| $[Z_{mn}]$ | moment-method interaction matrix |
| η | intrinsic impedance of free space |
| θ_i | incident angle of radar wave |
| θ_s | scattering angle of field |
| λ | radar wave length |
| Λ | surface wave length |
| σ | standard deviation of surface height |
| σ^0 | surface backscattering coefficient |
| ψ | angle between position vector and the surface normal vector at observation point |
| ψ' | angle between position vector and the surface normal vector at source point |

CHAPTER I.

INTRODUCTION

The investigation of radar scattering from the ocean surface is of interest for both military and purely scientific applications. The military is interested because the scattering from the surface results in radar image clutter which can mask the echo from a desired target. Understanding and predicting the radar scattering from the ocean surface may eventually lead to better methods to suppress the clutter or to correctly extract the target from the clutter. A purely scientific application is the use of spaceborne imaging radar as an oceanographic tool to investigate the features of the ocean surface such as current boundaries, temperature gradients, slicks, eddies, internal waves, surface waves and monitoring the pollution of the ocean, etc. The scattering characteristics must be understood to properly interpret the images.

No closed-form solution of Maxwell's equations exist to describe radar scattering from a rough surface such as the ocean. Thus, several approximate theories have been developed to solve the scattering problems over the last 40 years. Some examples are the small-perturbation method (or Bragg scattering) (Rice, 1951; Nieto-Vesperinas and Garcia, 1981), the Kirchhoff approximation (or physical optics) (Beckmann and Spizzichino, 1963), two-scale theories (Brown, 1978; McDaniel and Gorman, 1983; Rodriguez, 1989), phase perturbation approximation (Shen and Maradudin, 1980; Winebrenner and Ishimaru, 1985 a/b and Broschat, 1993), and full wave theories (Bahar, 1987). Each theory includes several approximations in their derivation that makes it applicable only to a limited class of surface roughness (e.g. roughness is small or the correlation length is large compared to the radar wavelength,) or within a specific range of angle of incidence. The actual ocean surface does not fall neatly into a region where an analytical theory is known to be applicable. Some attempts have been made to modify the existing theories to fit the actual ocean surface, but the validity of these modified theories

is still unknown, specially when the angle of incidence of the radar onto the surface is very large (near grazing incidence).

Numerical modeling has often been used to investigate the validity of approximate rough-surface scattering theories. Numerical methods used in this area include the moment method (Harrington, 1968 Lentz, 1974 and Axline 1978), the boundary element method (Kress, 1990 and Ingber, 1991), and the finite element method (Morgan, 1990 and Lou, 1990). The finite element method is usually used to solve differential equations in closed boundary problems. The moment method and the boundary element method are convenient for solving integral equations in closed or open boundary problems.

The most common numerical method used in rough-surface scattering problems is the moment method applied to integral equation formulations. The moment method calculations have often been referred to as the exact solution and used to investigate the validity of approximate theories (Chan, 1978; Chen, 1988; Thorsos, 1988; Thorsos, 1989; Chen, 1989; Rodriguez, 1992 and Kim, 1992). However, they are not actually closed form solutions and can only be applied under limited surface and illumination conditions. Finite computer resources limit the sizes of scatterers that can be modeled, and force approximations in the modeled geometry and electromagnetic illumination. For example, much larger surface areas will be illuminated than can be modeled on existing computer systems. Thus, the modeled surface must be artificially truncated, leading to nonphysical edge diffraction being predicted in the scattered field. The influence of this on the accuracy of the solution is strongly dependent on the incident angle and the size of the truncated section.

A commonly used technique to reduce the edge effects in moment-method calculations is the application of a tapered windowing function to the modeled electromagnetic field illuminating the surface. The windowing function falls off smoothly to negligible level at the ends of the truncated surface. Since the edges are not illuminated, the edge diffraction effects are greatly reduced. However, there are several limitations in the use of windowing functions. When a windowing function is applied, the modeled incident field no longer exactly represents the actual incident field, (in extreme cases, the windowed field is not even a valid solution of Maxwell's equations (Thorsos, 1988)). This

leads to an inaccurate prediction of the scattered field. Previous work has shown that the use of windowing functions is applicable only at angles of incidence less than about 60° to 80° , depending on the maximum computer resources available (Wetzel, 1977; Thorsos, 1988; Broschat, 1993 and Chen and Fung, 1985). Thus, this technique cannot be used at the largest incident angles.

Another method of avoiding edge effects in a moment method model of rough-surface scattering is to assume that the surface is periodic. Then only a single period of the surface must be numerically modeled, and the effects of the infinite surface appear as an infinite series in the integral equations describing the scattering (Twersky, 1956; Hessel and Oliver 1965; Jordan, 1979; Truang, 1981; Zaki, 1971; Kalhor, 1989 and Boag, 1989). Because the modeled surface is infinite, no edge-diffraction effects appear in the scattered fields. Unfortunately, no closed form solution to the infinite summation exists. In actual numerical computations, this summation must be truncated. This is equivalent to limiting the number of periods in the modeled surface. Rodriguez (1992) showed that the number of terms that must be maintained in the infinite summation depends strongly on the angle of incidence, with extremely large numbers required at large incident angles. Direct evaluation of these summations is computationally prohibitive.

In this work, the moment method is extended to allow the calculation of scattering from rough surfaces at small grazing angles using a periodic surface representation. The limitations of earlier periodic methods are overcome by deriving universal summations that are common to all elements in the moment method interaction matrix, thereby allowing the inclusion of a very large number of surface periods with little additional computational expense. An error analysis is performed to determine the optimal trade-off between accuracy and computational expense. The validity of the new technique is investigated by comparing its predicted scattering to the theoretically calculated scattering for the problems where a closed form solution exists. It is also compared with the predictions of the approximate scattering theories under conditions where they are known to be valid. The technique is then applied to random rough surfaces, and the validity of the approximate scattering theories is evaluated under various surfaces and illumination conditions.

CHAPTER II.

INTEGRAL EQUATIONS AND THE MOMENT METHOD

Introduction

This chapter gives a brief review of the moment method and of the integral equations typically used in the scattering problems. Scattering from perfectly conducting objects is usually described by the electrical field integral equation (EFIE) or the magnetic field integral equation (MFIE). The moment method is a numerical technique to solve general integro-differential equations. In this technique, the equation to be solved is approximated by a system of discrete linear equations that can be solved using standard techniques. The application of the technique to basic electromagnetic problems is given by Harrington (1967, 1968).

Electric Field Integral Equation (EFIE)

Scattering problems are conveniently described by integral equations based on the scatterer boundary conditions. Two of the most popular integral equations used to represent the scattering of time-harmonic electromagnetic fields are the electric field integral equation (EFIE) and the magnetic field integral equation (MFIE). The EFIE insures that the sum of the (known) incident and (unknown) scattered electric field meet the applicable boundary conditions on the surface of the scatterer and the MFIE insures the magnetic field meets its boundary conditions. In general, these are vector integral equations for which closed-form solutions exist only for very simple geometries. Thus, several approximate solutions have been developed for various scatterer geometries.

Unfortunately, the validity of many of these approximate theories has been difficult to confirm under many illumination conditions.

The electric field integral equation (EFIE) is based on the electric field boundary condition on the perfectly electric conducting surface of a scatterer; i.e. the total tangential electric field is zero. This boundary condition can be expressed as

$$\mathbf{E}_t = \hat{n} \times (\mathbf{E}^i + \mathbf{E}^s) = 0 \quad \text{on the surface } S \quad (2-1)$$

where \hat{n} is the normal unit vector on the surface, the subscript t indicates tangential components and the superscripts i and s denote the incident and scattered electric fields, respectively.

For the general scattering problem, the EFIE takes the form (Balanis, 1989; Rao, 1982)

$$j\frac{\eta}{k} \hat{n} \times \left[k^2 \iint_S \mathbf{J}_s(\mathbf{r}') G(\mathbf{r}, \mathbf{r}') ds' - \iint_S \nabla' \cdot \mathbf{J}(\mathbf{r}') \nabla' G(\mathbf{r}, \mathbf{r}') ds' \right] = \hat{n} \times \mathbf{E}_t \quad \text{on } S \quad (2-2)$$

where $\eta = \sqrt{\frac{\mu_0}{\epsilon_0}}$ is the intrinsic impedance of free space, $k = \omega \sqrt{\epsilon\mu} = \frac{2\pi}{\lambda}$ is the wave number, λ is the incident field wavelength, \mathbf{r} is the observation point vector, \mathbf{r}' is the source point vector, S is the surface of scatterer and $G(\mathbf{r}, \mathbf{r}')$ is the Green's function in three-dimensional form

$$G(\mathbf{r}, \mathbf{r}') = \frac{e^{-jkR}}{4\pi R} \quad (2-3)$$

where R is the distance between the observation point and the source point

$$R = |\mathbf{r} - \mathbf{r}'| = \sqrt{(x - x')^2 + (y - y')^2 + (z - z')^2} \quad (2-4)$$

Equation (2-2) can be solved to find the surface current density on the scatterer, and the scattered field can then be directly calculated from the surface currents using

$$\mathbf{E}^s(\mathbf{r}) = -j\mu\omega \int_S \mathbf{J}_s(\mathbf{r}') G(\mathbf{r}, \mathbf{r}') ds' + \frac{j}{\epsilon\omega} \nabla \int_S \nabla' \cdot \mathbf{J}_s(\mathbf{r}') G(\mathbf{r}, \mathbf{r}') ds' \quad (2-5)$$

Note that equation (2-2) is a vector integro-differential equation for the surface current.

Equation (2-5) can be greatly simplified for problems that depend only on two dimensions. For example, in the TM polarization problem in Figure 1, a uniform plane wave incidence on a two-dimensional conducting surface is described by

$$\mathbf{E}^i(\boldsymbol{\rho}) = \hat{\mathbf{a}}_z E_0 e^{jk(x \cos\theta_i + y \sin\theta_i)} \quad (2-6)$$

The scattering surface is defined by $y=f(x)$. Since the incident electric field has only a z-component the magnetic field has only x and y components and the induced current on surface in Figure 1 will have only a z-component: $\mathbf{J} = \hat{\mathbf{a}}_z J_z$. Equation (2-2) then reduces to

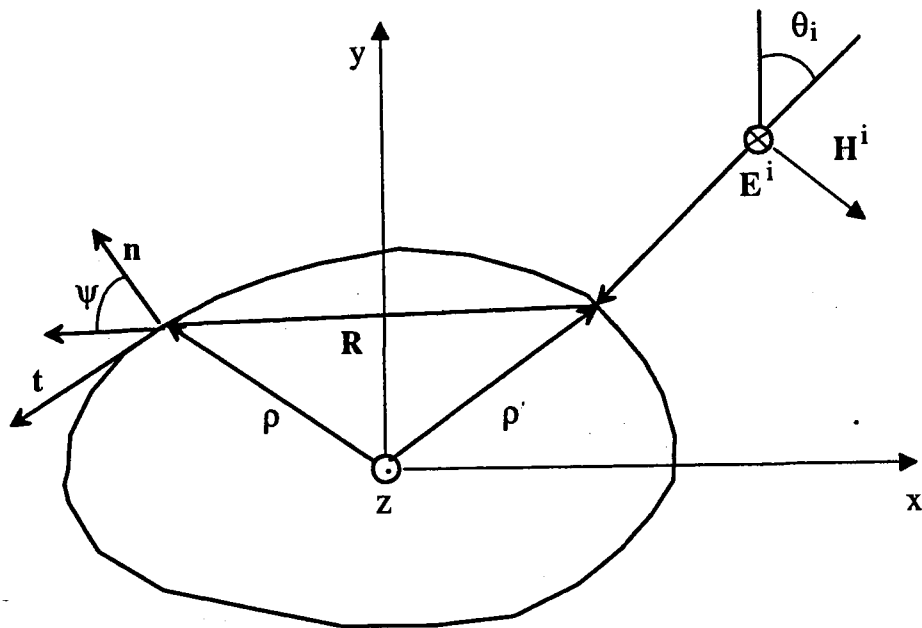


Figure 1. Geometry for two-dimensional scattering problems, TM polarization case.

$$\frac{k\eta}{4} \int_L J_z(\rho') H_0^{(2)}(kR) dl = E_z^i(\rho) \quad (2-7)$$

where L is the surface profile in the x - y plane and $H_0^{(2)}(kR)$ is the zero-order Hankel function of the second kind. Equation (2-7) is referred to as the two dimensional electric field integral equation for TM^z polarization. This equation is a scalar integral equation and can be directly solved by the moment method.

Magnetic Field Integral Equation (MFIE)

The magnetic field integral equation (MFIE) is based on the magnetic field boundary condition at the conducting surface; i.e. the magnitude of the total tangential magnetic field at the surface is equal to the magnitude of the surface current density induced on the surface. This boundary condition can be expressed as

$$\mathbf{J}_s = \hat{n} \times \mathbf{H} = \hat{n} \times (\mathbf{H}^i + \mathbf{H}^s) \quad \text{on the surface } S \quad (2-8)$$

where \hat{n} is the normal vector unit to the surface, the subscript s indicates the surface current density, the superscript i indicates the incident wave, and superscript s indicates the scattered wave. For the general scattering problem the MFIE takes the form (Balanis, 1989; Mittra, 1973)

$$\frac{\mathbf{J}_s(\mathbf{r})}{2} - \hat{n} \times \iint_{S-\Delta S} \mathbf{J}_s(\mathbf{r}') \times \nabla' G(\mathbf{r}, \mathbf{r}') ds' = \hat{n} \times \mathbf{H}^i(\mathbf{r}) \quad (2-9)$$

The integration region $S-\Delta S$ indicates the principle-value evaluation of the integral around the singularity at $\mathbf{r} = \mathbf{r}'$. This equation is also a vector integro-differential equation for the surface current. Its form can be simplified in two-dimensional cases for both TM and TE polarizations.

Again consider a TM uniform plane wave illuminating upon a two-dimensional surface as in Figure 1. The magnetic field can be expressed as

$$\mathbf{H}^i(\rho) = H_0(\hat{a}_x \cos \theta_i - \hat{a}_y \sin \theta_i) e^{jk(x \cos \theta_i + y \sin \theta_i)} \quad (2-10)$$

Again, since the electric current density induced on the surface of the scatterer has only a z component, equation (2-9) can be reduced to a scalar integral equation:

$$\frac{J_z(\rho)}{2} + j\frac{k}{4} \int_{L-\Delta l} J_z(\rho') \cos \psi H_1^{(2)}(kR) dl = H_t^i(\rho) \quad (2-11)$$

where $H_1^{(2)}(kR)$ is the first-order Hankel function of the second kind, H_t^i is the tangential component of the incident magnetic field at the observation point on the surface of the scatterer and ψ is the angle between the distance vector \mathbf{R} and the normal vector at the observation point \hat{n} , shown in Figure 1:

$$\cos \psi = \hat{a}_R \cdot \hat{n} \quad (2-12)$$

Equation (2-11) is a scalar integral equation and can be easily solved by the moment method.

A two-dimensional MFIE for TE polarization can be derived for the case in Figure 2. The incident magnetic field has only a z-component and the induced current is along the surface profile (J_t). The simplified integral equation for this case is

$$\frac{J_t(\rho)}{2} + j\frac{k}{4} \int_{L-\Delta l} J_t(\rho') \cos \psi' H_1^{(2)}(kR) dl' = -H_z^i(\rho) \quad (2-13)$$

where ψ' is the angle between the distance vector and the normal vector at the observation point and shown in Figure 2.

As mentioned before, the EFIE is most convenient for modeling TM polarization while the MFIE is commonly used with TE polarization. However, the moment matrix of the MFIE is diagonally dominant. This characteristic allows the MFIE matrix equations to be quickly solved by iterative methods, and is not shared by EFIE moment method implementations. Thus, the MFIE must be considered for solving very large scattering TM polarization scattering problems.

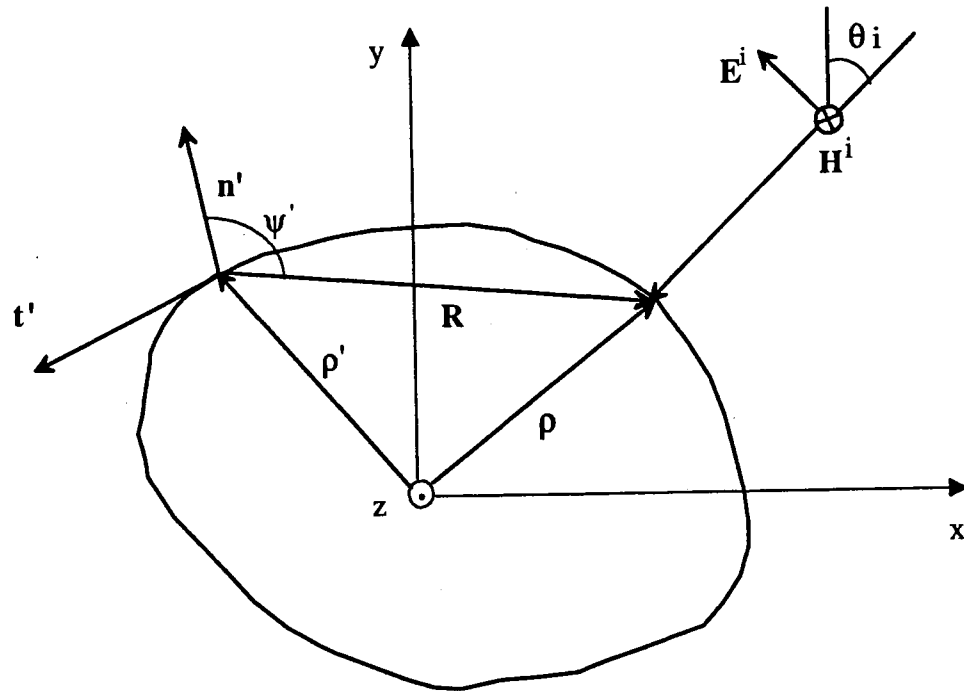


Figure 2. Geometry for two-dimensional scattering problems, TE polarization case.

Moment Method with Point Matching

The moment method is used to find approximate solutions to general integro-differential equations of the form

$$L[f(\mathbf{R})] = g(\mathbf{R}) \quad (2-14)$$

where L is a linear operator, f is the unknown function to be determined and g is a known function. The method of the moments begins by approximating the unknown function by a linear combination of known basis functions $N_i(\mathbf{R})$ in the form

$$f(\mathbf{R}) \approx \sum_{i=1}^N \alpha_i N_i(\mathbf{R}) \quad (2-15)$$

where the α_i are coefficients to be determined. Substitution of (2-15) into (2-14) and use of the linearity of the operator $L[]$ yields

$$\sum_{i=1}^N \alpha_i L[N_i(\mathbf{R})] \approx g(\mathbf{R}) \quad (2-16)$$

The residual of the approximate solution is now defined as

$$Res(\mathbf{R}) = \sum_{i=1}^N \alpha_i L[N_i(\mathbf{R})] - g(\mathbf{R}) \quad (2-17)$$

The values of the coefficients α_i must be chosen so the residual is minimized across domain of the problem. The moment method uses the method of weighted residuals. The weighted residuals are obtained by taking inner product of the residual function and N weighting functions $w_j(\mathbf{R})$

$$\langle w_j(\mathbf{R}), Res(\mathbf{R}) \rangle = \int_{\Omega} w_j(\mathbf{R}) Res(\mathbf{R}) d\Omega \quad (2-18)$$

Setting the weighted residuals equal to zero and using the linearity of the inner product yields the general moment equation:

$$\sum_{i=1}^N \alpha_i \int_{\Omega} w_j(\mathbf{R}) L[N_i(\mathbf{R})] d\Omega = \int_{\Omega} w_j(\mathbf{R}) g(\mathbf{R}) d\Omega \quad (2-19)$$

Equation (2-19) represents N linear equations and N unknowns that can be solved for the α_i unknown coefficients using standard linear algebra techniques.

Basis Functions

Ideally, the basis functions should be chosen so that they naturally approximate the unknown function and meet the required boundary conditions. Also, they should be chosen to minimize the computational effort [Ney, 1985; Sarkar, 1981]. There are an infinite number of sets of possible basis functions. These sets may be divided into two general groups, entire domain basis functions and subdomain basis functions. Entire

domain basis functions exist over the entire domain (an example of an entire domain basis-function set is a truncated Fourier series expansion). Individual subdomain basis functions only exist over a part of the domain, and the entire set of basis functions is required to describe the unknown function over the entire domain. In electromagnetic scattering problems, subdomain basis functions usually give a better approximation of the solution, and are much more computationally efficient. Thus, they are almost exclusively used (Andreasen, 1964; Harrington, 1968 and Axline, 1978).

One of the simplest expansions is the use of pulse basis functions as shown in Figure 3. In this, the surface is divided into a number of very small segments (in two dimensional problems) and the current density on each segment is assumed to be a constant. The i th basis function is therefore equal to 1 on the i th segment and equal to 0 on the other sections

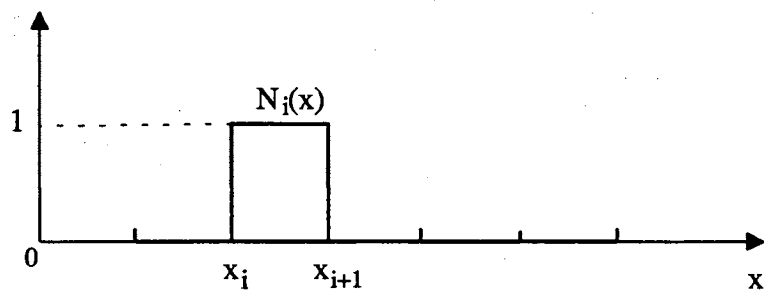
$$N_i(x) = \begin{cases} 1 & x_i \leq x \leq x_{i+1} \\ 0 & \text{otherwise} \end{cases} \quad i=1, 2, 3, \dots, N \quad (2-20)$$

where N is the number of segments and x_i is the end-point of a segment.

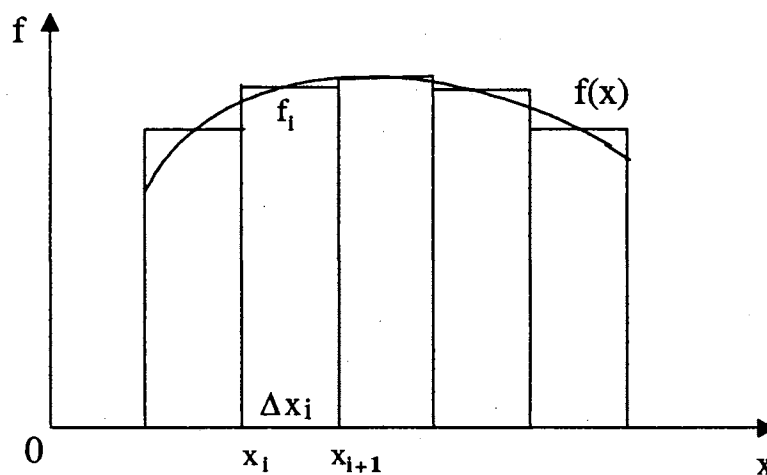
This basis function expansion yields a piecewise step approximation to the unknown function on the whole surface, as shown in Figure 3-b. The pulse function is the crudest subdomain basis function, often requiring more basis functions to adequately describe the unknown function than a more complicated basis function set would need. This increases the order of the linear system that must be solved in equation (2-19), requiring more computation. However this is compensated because, due to the simplicity of the function, numerical integration can often be avoided in the evaluation of the linear operator or the inner product.

Many other basis functions have been used in moment method treatments of the scattering problem. These include piecewise-linear functions (Harrington, 1968; Chen, 1991), sinc functions [Herrmann, 1990], piecewise sinusoid functions and truncated cosine functions [Balanis, 1989]. All of these basis functions more closely approximate the shape of the unknown current, thereby reducing the number basis functions needed to adequately

model a region, but at the expense of much greater computational complexity. Previous works have shown that the benefits gained using more complicated basis functions in surface scattering problems are marginal, at best (Burke and Poggio, 1977).



a. Pulse basis function



b. Function representation.

Figure 3. A set of pulse basis functions used for representing an arbitrary function $f(x)$.

Choice of Basis and Weighting Functions

Ideally, the basis and weighting functions should be chosen so that the residual on the entire boundary and the computational complexity are minimized (Ney, 1985 and Sultan, 1985). A commonly used approach is the point-matching method combined with the pulse basis function. In this, the weighting functions are defined as Dirac delta functions

$$w_j = \delta(\mathbf{R} - \mathbf{R}_j) \quad (2-21)$$

This approach minimizes the computational complexity (the inner products are reduced to the evaluation the operand at discrete matching points), and forces the residuals to be zero at the matching points.

This method can be applied to the integral equations derived in the previous sections. For the EFIE describing the two dimensional TM polarization case in Equation (2-7), the unknown function is the current density on the surface J_z , the linear operator $L(\)$ is

$$L(\) = \frac{k\eta}{4} \int_L H_0^{(2)}(kR) dl, \quad (2-22)$$

and g is tangential component of the incident electric field on the surface. Substituting (2-22) into (2-19) and using pulse-basis point-matching equation (2-19) is reduced to

$$\frac{k\eta}{4} \sum_{n=1}^N J_n \int_{\Delta l_n} H_0^{(2)}(kR) dl = E_z^i(\rho_m) \quad (2-23)$$

Scanning the observation point from segment 1 to N yields the moment matrix equation as

$$[Z_{mn}] [J_n] = [V_m] \quad (2-24)$$

where $V_m = E_z^i(\rho_m)$ is the illumination electric field tangential component at the center of the m th segment and Z_{mn} is defined as

$$Z_{mn} = \frac{k\eta}{4} \int_{\Delta l_n} H_0^{(2)}(kR) dl \quad (2-25)$$

There is no simple closed form expression for the integral (2-25) in the general case, but accurate approximations are obtained if the integration length Δl_m is small compared to the wavelength. If the observation point and the source point coincide ($m=n$), the Hankel function in (2-25) has an integrable singularity and that can be approximately evaluated analytically [Balanis, 1989]:

$$Z_{mm} \approx \frac{k\eta}{4} \Delta l_n H_0^{(2)} \left(1 - j \frac{2}{\pi} \ln \frac{\gamma k \Delta l_m}{4e} \right) \quad (2-26)$$

The nondiagonal element of Z can be approximately evaluated as

$$Z_{mn} \approx \frac{k\eta}{4} \Delta l_n H_0^{(2)}(kR_{mn}) \quad (2-27)$$

Using the terms in equations (2-26) and (2-27), equation (2-24) can be solved for current coefficients J_z giving the approximate current distribution on the surface. Implementation of the moment method using the MFIE with pulse basis functions and point matching is quite similar to the implementation of the EFIE, as outlined by Harrington (1968).

CHAPTER III

APPLICATION OF MOMENT METHOD TO PERIODIC SURFACES

Introduction

In this chapter, the periodic surface models describing the scattering from periodic surfaces for TM and TE polarization wave are derived. The moment method is extended to overcome the drawbacks of traditional application to periodic problems. A set of universal summations are derived based on a Taylor expansion series for Hankel functions to eliminate redundant computations involved in the infinite summation required to compute the elements of the moment method interaction matrix. These universal summations can greatly reduce the computational time involved in the construction of the moment matrix. A time analysis in the next chapter shows that, under many realistic conditions, application of the method to a periodic surface which includes a great number of periodic sections requires only slightly more computational time than the corresponding traditional moment method applied to a single surface section, while providing a dramatic reduction in the edge effects in the calculated surface current.

Model of Integral Equations for Periodic Structure

EFIE for TM Polarization

Consider a periodic surface of arbitrary smooth cross section as shown in Figure 4. The surface is periodic in the x direction with a period L and uniform along the y coordinate. A uniform TM^z polarized plane is incident on the periodic surface at an angle θ_i . The

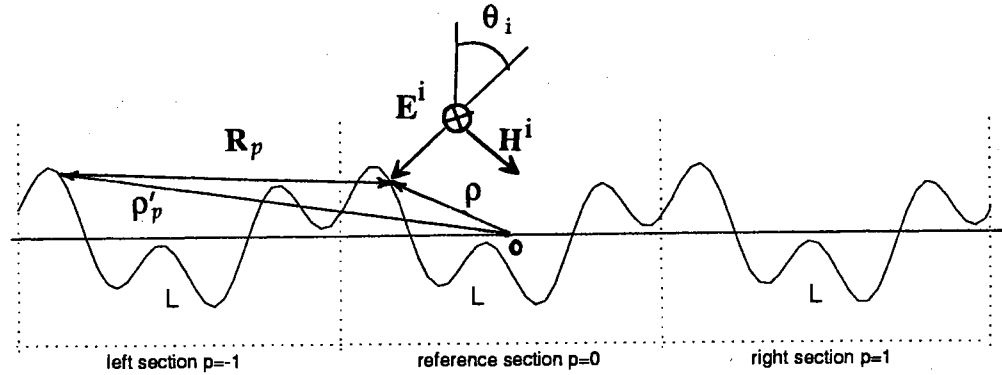


Figure 4. General problem of scattering from a periodic surface.

incident field is described by (2-6). The EFIE for the periodic structure can be rewritten from (2-7) :

$$\frac{k\eta}{4} \sum_{p=-\infty}^{\infty} \int_{L_p} J(\rho'_p) H_0^{(2)}(kR_p) dl = E_0^i(\rho) \quad (3-1)$$

where p denotes the p th periodic section, L_p is the surface over the p th period, ρ'_p is the source vector at the p th period and the R_p is the distance between the observation point and the source point on the p th periodic section, shown in Figure 4. Because the incident field is uniform, the magnitudes of the induced current at the same point on the periodic sections are identical, and the phase of the current will be shifted by an angle determined by the period and angle of incidence [Green, 1970]. We refer to the center periodic section as the reference section. The subscript 0 is used to represent the reference section and the subscript p is used to represent the p th periodic section. The current on the different periodic sections can be expressed based on the reference section current as

$$J_z(\rho') = J_0(\rho') \quad \text{on the reference section} \quad (3-2)$$

$$J_z(\rho'_p) = J_z(\rho' + pL) = J_0(\rho')e^{jkpL \sin\theta_i} \quad \text{on the } p\text{th section} \quad (3-3)$$

where $0 \leq \rho' \leq L$. Substituting (3-2) and (3-3) into (3-1), the EFIE for the periodic surface with TM^z polarization is obtained as

$$\frac{k\eta}{4} \int_{L_0} J_0(\rho') \sum_{p=-\infty}^{\infty} e^{jkpL \sin\theta_i} H_0^{(2)}(kR_p) dl = E_0^i(\rho) \quad (3-4)$$

where L_0 is the surface of the reference section. Equation (3-4) includes an infinite summation that has no general closed-form evaluation. Thus, it must be evaluated numerically. Because of its slow convergence, it must be truncated at large values of M (equivalent to using a finite number of periodic sections).

MFIE for TM Polarization

Again referring to Figure 4, the MFIE for TM^z polarization for the periodic surface is expressed as

$$\frac{J_z(\rho)}{2} + j\frac{k}{4} \sum_{p=-\infty}^{\infty} \int_{L_p} J(\rho'_p) \cos\psi_p H_1^{(2)}(kR_p) dl = H_t^i(\rho) \quad (3-5)$$

where ψ_p is the angle between the distance vector \mathbf{R}_p and the normal vector at the observation point, and R_p is the distance between the observation point at the reference section and the source point at the p th periodic section, shown in Figure 4. Note that the principal value evaluation of the integral must be used at the singularity at $\rho'_p = \rho$ when the source and the reference surface section coincide ($R=0$). Substituting the periodic current (3-2) and (3-3) into (3-5), the MFIE for the periodic surface with TM^z polarization becomes

$$\frac{J_0(\rho)}{2} + j\frac{k}{4} \int_{L_0} J_0(\rho') \sum_{p=-\infty}^{\infty} e^{jkpL \sin\theta_i} \cos\psi_p H_1^{(2)}(kR_p) dl = H_t^i(\rho) \quad (3-6)$$

$$\frac{J_0(\rho)}{2} + j\frac{k}{4} \int_{L_0} J_0(\rho') \sum_{p=-\infty}^{\infty} e^{jkpL \sin \theta_i} \cos \psi_p H_1^{(2)}(kR_p) dl = H_t^i(\rho) \quad (3-6)$$

The subscript t indicates the tangential component of the incident wave. This equation also includes an infinite summation that has no general closed form evaluation.

MFIE for TE Polarization

Consider an arbitrary smooth periodic surface which is the same as shown in Figure 4. A uniform TE^Z polarized plane wave

$$\mathbf{H}^i(\rho) = \hat{a}_z H_0 e^{jk(x \cos \theta_i + y \sin \theta_i)} \quad (3-7)$$

is incident on the periodic surface at an angle θ_i . The MFIE for the periodic structure can be rewritten based on (2-13) as

$$\frac{J_t(\rho)}{2} + j\frac{k}{4} \sum_{p=-\infty}^{\infty} \int_{L_p} J_t(\rho') \cos \psi'_p H_1^{(2)}(kR_p) dl' = -H_z^i(\rho) \quad (3-8)$$

where p denotes the pth periodic section and ψ'_p is the angle between the distance vector \mathbf{R}_p and the normal vector \mathbf{n}'_p at the source point on the pth section. Here the principle value evaluation of the integral has been used at the singularity at $\rho' = \rho$ when the source and the reference surface section coincide ($R=0$). Again substituting the periodic current (3-2) and (3-3) into (3-8), the MFIE for the periodic surface at TE^Z polarization can be rewritten as

$$\frac{J_t(\rho)}{2} + j\frac{k}{4} \int_{L_0} J_{t_0}(\rho') \sum_{p=-\infty}^{\infty} e^{jkpL \sin \theta_i} \cos \psi'_p H_1^{(2)}(kR_p) dl = -H_z^i(\rho) \quad (3-9)$$

where J_{t_0} is the tangential current on the reference section.

Moment Method with Periodic Surface

The moment method using pulse basis functions and point matching is now applied to equations (3-4), (3-6) and (3-9) to develop the moment equations for a periodic surface at various polarizations.

EFIE PS Model for TM polarization

In equation (3-4), the unknown function (current $J_0(\rho')$) is confined to the region $0 \leq \rho' \leq L$. The region is now divided into N segments and pulse basis functions are used on each segment. The matching points are at the center of the each segment. The moment method representation then becomes

$$[Z_{mn}][J_n] = [E_m] \quad (3-10)$$

where $[J_n]$ is the $N \times 1$ unknown current density vector, $[E_m]$ is the $N \times 1$ known source of the incident field vector on the reference section defined in (2-6) and $[Z_{mn}]$ is a $N \times N$ moment coefficient matrix. Using the approximate evaluation of integrals as in equations (2-26) and (2-27), the elements of the matrix Z_{mn} are

$$Z_{mn} = \frac{k\eta}{4} \Delta l_n \sum_{p=-\infty}^{\infty} e^{jkpL \sin \theta_i} H_0^{(2)}(kR_p) \quad m \neq n \quad (3-11)$$

$$Z_{mm} = \frac{k\eta}{4} \Delta l_m \left[\left(1 - j \frac{2}{\pi} \ln \frac{\gamma k \Delta l_m}{4e} \right) + \sum_{\substack{p=-\infty \\ p \neq 0}}^{\infty} e^{jkpL \sin \theta_i} H_0^{(2)}(kR_p) \right] \quad m = n \quad (3-12)$$

Equation (3-11) gives the off-diagonal elements and (3-12) gives the diagonal elements of the matrix. The first term in (3-12) is due to the integrable singularity in the Hankel function when the distance is zero. Solving equations (3-10) gives the approximate solution of the current density on the reference section. The current density on the other sections can then be obtained using (3-3).

MFIE PS Model for TM polarization

We now apply the moment method to the MFIE for a periodic surface at TM polarization. The reference section is again divided into N segments and pulse basis functions with point matching at the segment center are again used. The moment matrix equations now become

$$[Z_{mn}][J_n] = [H_m] \quad (3-13)$$

where $[J_n]$ is the $N \times 1$ unknown current density array, $[H_m]$ is the $N \times 1$ known tangential component of the incident magnetic field (2-10) at the matching point, and $[Z_{mn}]$ is a $N \times N$ moment coefficient matrix whose elements are given by

$$Z_{mn} = j\frac{k}{4} \Delta l_n \sum_{p=-\infty}^{\infty} \cos \psi_p e^{jkpL \sin \theta_i} H_1^{(2)}(kR_p) \quad m \neq n \quad (3-14)$$

$$Z_{mm} = \frac{1}{2} + j\frac{k}{4} \Delta l_m \sum_{\substack{p=-\infty \\ p \neq 0}}^{\infty} \cos \psi_p e^{jkpL \sin \theta_i} H_1^{(2)}(kR_p) \quad m = n \quad (3-15)$$

Solving (3-13) again yields the approximate solution of the current density on the reference region.

MFIE PS Model for TE polarization

We now apply the moment method to the MFIE for a periodic surface at TE polarization. The reference section is again divided into N segments and pulse basis functions with point matching at the segment center are again used. The moment matrix equations now become

$$[Z_{mn}][J_t] = [H_m] \quad (3-16)$$

where $[J_t]$ and $[H_m]$ are the $N \times 1$ unknown tangential current density array and known incident magnetic field (3-7) at the matching point respectively and $[Z_{mn}]$ is a $N \times N$ moment matrix whose elements are given by

$$Z_{mn} = j\frac{k}{4} \Delta l_n \sum_{p=-\infty}^{\infty} \cos \psi'_p e^{jkpL \sin \theta_i} H_1^{(2)}(kR_p) \quad m \neq n \quad (3-17)$$

$$Z_{mm} = \frac{1}{2} + j\frac{k}{4} \Delta l_m \sum_{\substack{p=-\infty \\ p \neq 0}}^{\infty} \cos \psi'_p e^{jkpL \sin \theta_i} H_1^{(2)}(kR_p) \quad m = n \quad (3-18)$$

Solving (3-16) yields the approximate solution of the tangential current component density on the reference section.

Universal Summations

The moment method analysis of the TM^z scattering from a periodic rough surface has been implemented on an IBM RS6000 320 computer. As expected, it was found that the infinite summations converge very slowly, especially at extreme incident angles. Tests showed that converging the terms to an arbitrary tolerance wasted computational time on terms where the series evaluates to a very small number. Instead, truncating the series at arbitrary value $p=M$ (i.e. the summation extends from $-M$ to M , so $2M+1$ periodic sections are included in the modeled surface) was found to give best the trade-off between accuracy and computational effort. The greater M , the farther the edge is physically removed from the reference section thereby reducing the edge effects. The number of sections needed depends strongly on angle of incidence. Rodriguez et al. (1992) used $M=1$, which proved adequate at angles of incidence of less than about 60° . However, at near-grazing angles, far more sections must be used. To demonstrate this, the scattering of a uniform plane wave incident on an infinite flat plane (which is a special-case periodic surface) was modeled, as shown in Figure 5. The incident angle was 88° and the surface period was set at $L=10\lambda$. Figure 6 shows the current distribution along the surface calculated by the moment method with $M=0, 1, 10, 100$ and 10000 . The exact current distribution is also shown in the figure for comparison. The figure clearly shows the effects of the edges and the dependence on M . Unfortunately, a very large M ($\sim 10,000$) is

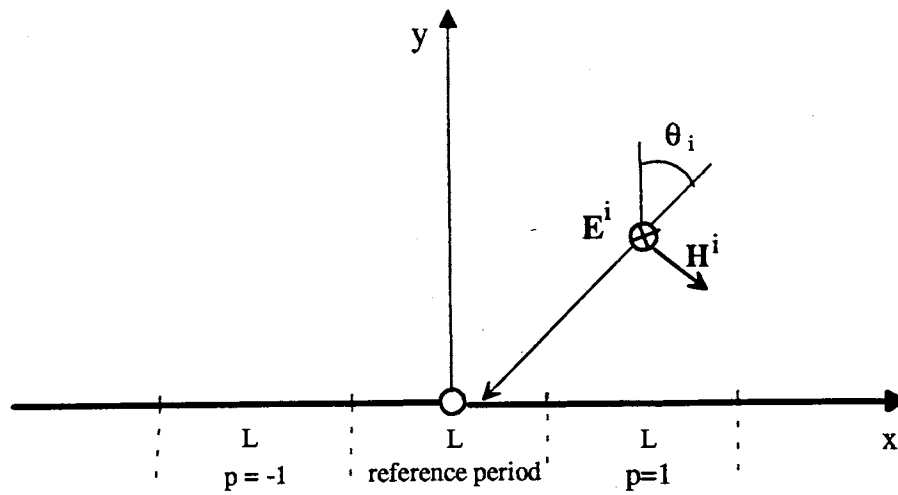


Figure 5. Geometry for an infinite plane scattering problem, TM polarization case.

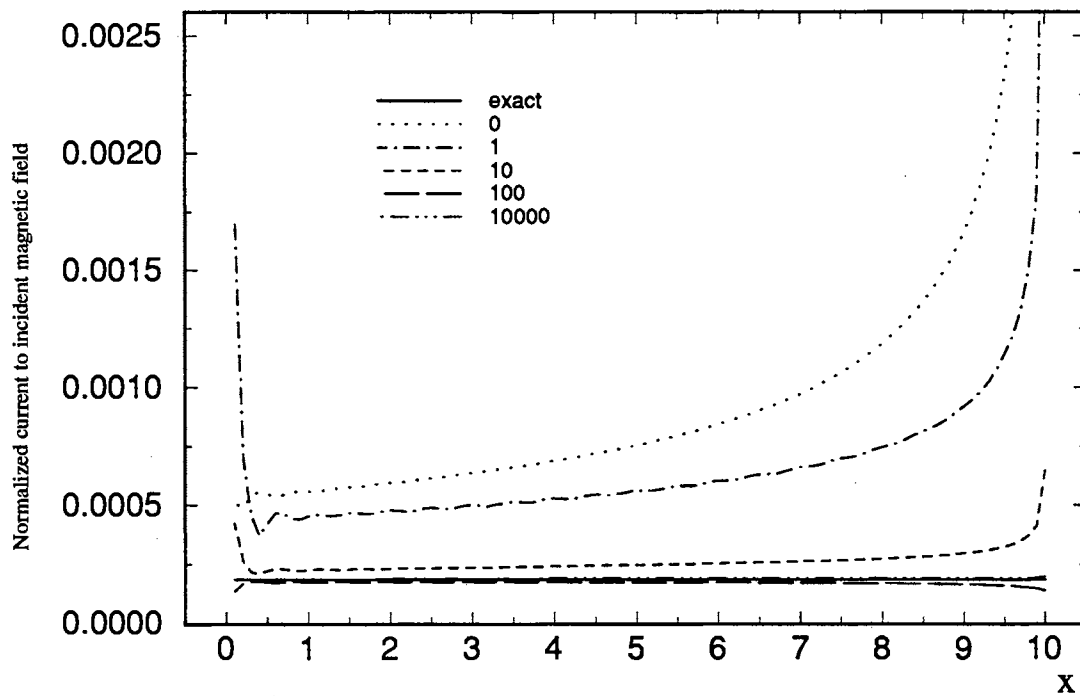


Figure 6. Current distributions for PS model with various periodic sections M . Scattering from an infinite flat plane, TM polarization, $\theta_i=88$ degree.

required to reduce the edge effects to an acceptable level in this problem.

Directly summing 10,000 terms in the evaluation of each matrix element in (3-8), (3-9), (3-10) and (3-11) is cost prohibitive. Instead, a set of universal summations, similar to those used by Silvester (1969) for the application of the finite element method to potential problems, were determined. Combining the results of the universal summations with the much smaller portions of the original summations which are unique to each element leads to a much more efficient evaluation of the matrix elements.

EFIE TM Polarization

We first consider the evaluation of the summations in (3-11) and (3-12). When the source point is far from the reference section ($|pL| \gg |y - y'|$), the distance between source and observation points can be approximated by

$$\begin{aligned} R_p = |\rho - \rho'_p| &= \sqrt{[x - (x' + pL)]^2 + (y - y')^2} & (3-19) \\ &\approx (x' + pL) - x = pL(1 + \frac{x' - x}{pL}) & p > 0 \\ &\approx -(x' + pL) + x = -pL(1 + \frac{x' - x}{pL}) & p < 0 \end{aligned}$$

For large arguments, the Hankel function in (3-11) and (3-12) can be replaced by its asymptotic form of

$$H_0^{(2)}(x) \approx \sqrt{\frac{2}{\pi x}} e^{-j(x - \frac{\pi}{4})} \quad x \rightarrow \infty \quad (3-20)$$

When $p > 0$, using (3-19) and the Taylor expansion series

$$\frac{1}{\sqrt{1 + \delta x}} = 1 - \frac{1}{2}\delta x + \frac{3}{8}\delta x^2 - \frac{15}{48}\delta x^3 + \dots, \quad (3-21)$$

the Hankel function in (3-20) for large argument ($p > 0$) can be approximated by

$$\begin{aligned}
H_0^{(2)}(kR_{p^+}) &\equiv \sqrt{\frac{2}{\pi k p L (1 + \Delta x / p L)}} e^{-jk(pL + \Delta x - \frac{\pi}{4})} \\
&= \sqrt{\frac{2}{\pi k p L}} e^{-j(k\Delta x - \frac{\pi}{4})} e^{-jk p L} \left(1 - \frac{1}{2} \frac{\Delta x}{p L} + \frac{3}{8} \left(\frac{\Delta x}{p L}\right)^2 - \frac{15}{48} \left(\frac{\Delta x}{p L}\right)^3 + \dots\right)
\end{aligned} \tag{3-22}$$

where p^+ denotes the sections to the right of the reference section ($p > 0$) and $\Delta x = x' - x$. Letting p^- represent the left side sections ($p < 0$) and $q = -p > 0$, the Hankel function for large argument can be rewritten as

$$\begin{aligned}
H_0^{(2)}(kR_{p^-}) &\equiv \sqrt{\frac{2}{\pi k q L (1 - \Delta x / q L)}} e^{-jk(-qL - \Delta x - \frac{\pi}{4})} \\
&= \sqrt{\frac{2}{\pi k q L}} e^{-j(-k\Delta x - \frac{\pi}{4})} e^{jk q L} \left(1 + \frac{1}{2} \frac{\Delta x}{q L} + \frac{3}{8} \left(\frac{\Delta x}{q L}\right)^2 + \frac{15}{48} \left(\frac{\Delta x}{q L}\right)^3 + \dots\right)
\end{aligned} \tag{3-23}$$

p_0 is defined as the threshold such that when $|p| \geq p_0$, all approximations used in deriving (3-22) and (3-23) are valid. The infinite summation can now be divided into three parts: the left part with $p < p_0$, the center part with $-p_0 \leq p \leq p_0$ and the right part with $p > p_0$. Combining the summation for the left and right part and using (3-22) and (3-23), the portion of the summation where $|p| > p_0$ reduces to

$$\sum_{p=p_0}^M \left(e^{jk p L \sin \theta_i} H_0^{(2)}(kR_{p^+}) + e^{-jk p \sin \theta_i} H_0^{(2)}(kR_{p^-}) \right) = (S^r + S^l) \tag{3-24}$$

where S^r and S^l are

$$S^r = \sqrt{\frac{2}{\pi k L}} e^{-j(k\Delta x - \frac{\pi}{4})} \left(S_0^r - \frac{1}{2} S_1^r \Delta x + \frac{3}{8} S_2^r \Delta x^2 - \frac{15}{48} S_3^r \Delta x^3 + \dots \right) \tag{3-25}$$

$$S^l = \sqrt{\frac{2}{\pi k L}} e^{j(k\Delta x + \frac{\pi}{4})} \left(S_0^l + \frac{1}{2} S_1^l \Delta x + \frac{3}{8} S_2^l \Delta x^2 + \frac{15}{48} S_3^l \Delta x^3 + \dots \right) \tag{3-26}$$

S_v^r and S_v^l $v=0,1,2 \dots$, are hereafter termed universal summations for the right and left sections respectively. They are given by

$$S_v^r = \sum_{p=p_0}^M e^{-jkpL(1-\sin\theta_i)} \frac{1}{\sqrt{p} p^v} \quad v = 0, 1, 2, \dots \quad (3-27)$$

$$S_v^l = \sum_{p=p_0}^M e^{-jkpL(1+\sin\theta_i)} \frac{1}{\sqrt{p} p^v} \quad v = 0, 1, 2, \dots \quad (3-28)$$

The universal summations (3-27) and (3-28) are independent of the geometry of the problem and can be used for all elements in the matrix. Thus, these summations must only be evaluated once. Note that the universal summations are only dependent on the incident angle and the order of the Taylor series used. Also note that care must be taken in selecting L and θ_i so that the exponentials in (3-27) and (3-28) do not evaluate to 1. In this case the S_0^l and S_0^r summations do not converge.

We now define S^c to be the summation of the center terms where $|p| \leq p_0$

$$S^c = \sum_{p=-p_0}^{p_0} e^{jkL\sin\theta_i} H_0^{(2)}(kR_p) \quad (3-29)$$

Note that this summation requires exact evaluation of the Hankel functions and can dominate the computational effort if p_0 is large. Using (3-27) through (3-29), (3-11) and (3-12) can be reduced to the concise form

$$Z_{mn} = \Delta l_n \frac{k\eta}{4} (S^l + S^c + S^r) \quad (3-30)$$

When $m=n$, equation (3-29) must be modified slightly to include the contribution of the singularity in the integral when the source and observation points are co-located (compare with equation (3-12)). The universal summations greatly reduce the redundant computation, so the CPU time for the calculation of the matrix elements by (3-30) is much less than when evaluating (3-11) and (3-12) directly.

MFIE TM Polarization

Universal summations can also be determined for the application the moment method to the MFIE for periodic surfaces in equation. (3-17) and (3-18). For large arguments, the first-order Hankel function can be replaced by its asymptotic form

$$H_1^{(2)}(x) \approx \sqrt{\frac{2}{\pi x}} e^{-j\left(x - \frac{3\pi}{4}\right)} \quad x \rightarrow \infty \quad (3-31)$$

Also,

$$\cos \psi_p = \mathbf{n} \cdot \mathbf{a}_{R_p} \quad (3-32)$$

For large R_p

$$\mathbf{a}_{R_p} = \frac{\mathbf{a}_x(x - x' - pL) + \mathbf{a}_y(y - y')}{\sqrt{(x - x' - pL)^2 + (y - y')^2}} \approx -\frac{p}{|p|} \mathbf{a}_x \quad |pL| \gg |y - y'| \quad (3-33)$$

and

$$\mathbf{n} = \frac{\mathbf{a}_y - \mathbf{a}_x f'_s(x)}{\sqrt{1 + [f'_s(x)]^2}} \quad (3-34)$$

where the $f_s(x)$ defines the surface profile. Thus, (3-32) can be approximated by

$$\cos \psi_p \approx \frac{p}{|p|} \frac{f'_s(x)}{\sqrt{1 + [f'_s(x)]^2}} \quad |pL| \gg |y - y'| \quad (3-35)$$

Using (3-19) and the Taylor expansion series (3-21), the Hankel function (3-31) for large arguments can be approximated by

$$H_1^{(2)}(kR_p) = \sqrt{\frac{2}{\pi k p L}} e^{-j\left(k\Delta x - \frac{3\pi}{4}\right)} e^{-jk p L} \left(1 - \frac{1}{2} \frac{\Delta x}{pL} + \frac{3}{8} \left(\frac{\Delta x}{pL}\right)^2 - \frac{15}{48} \left(\frac{\Delta x}{pL}\right)^3 + \dots\right) \quad (3-36)$$

when $p > 0$ and

$$H_1^{(2)}(kR_{p^-}) = \sqrt{\frac{2}{\pi k q L}} e^{-j\left(-k\Delta x - \frac{3\pi}{4}\right)} e^{jk q L} \left(1 + \frac{1}{2} \frac{\Delta x}{qL} + \frac{3}{8} \left(\frac{\Delta x}{qL}\right)^2 + \frac{15}{48} \left(\frac{\Delta x}{qL}\right)^3 + \dots\right) \quad (3-37)$$

when $p < 0$ and $q = -p$. The summations of (3-14) and (3-15) are also divided into three parts, so the matrix elements are given by

$$Z_{mn} = \Delta l_n \frac{jk}{4} (S^l + S^c + S^r) \quad (3-38)$$

where S^r, S^l represent the summations for the right and the left sections respectively, and are given by

$$S^r = \cos \psi_{p^+} \sqrt{\frac{2}{\pi k L}} e^{-j\left(k\Delta x - \frac{3\pi}{4}\right)} \left(S_0^r - \frac{1}{2} S_1^r \Delta x + \frac{3}{8} S_2^r \Delta x^2 - \frac{15}{48} \Delta x^3 + \dots\right) \quad (3-39)$$

and

$$S^l = -\cos \psi_{p^-} \sqrt{\frac{2}{\pi k L}} e^{j\left(k\Delta x + \frac{3\pi}{4}\right)} \left(S_0^l + \frac{1}{2} S_1^l \Delta x + \frac{3}{8} S_2^l \Delta x^2 + \frac{15}{48} \Delta x^3 + \dots\right) \quad (3-40)$$

where S_v^r and $S_v^l, v = 0, 1, 2, 3, \dots$ are the universal summations given in (3-27) and (3-28). S^c is the summation of the center sections, and must be evaluated directly:

$$S^c = \sum_{p=-p_0}^{p_0} e^{jkL \sin \theta_i} H_1^{(2)}(kR_p) \cos \psi_p \quad (3-41)$$

where

$$\cos \psi_p = \frac{(y - y') - (x - x' - pL) f'_s(x)}{\sqrt{(x - x' - pL)^2 + (y - y')^2} \sqrt{1 + [f'_s(x)]^2}} \quad (3-42)$$

When $m=n$, equation (3-15) is used for the center summation.

MFIE TE Polarization

The universal summations derived for TM^z polarization scattering can also be used in the MFIE moment method for TE^z polarization. Since the development is very similar to that for the MFIE TM case, only the final result is given. Equations (3-17) and (3-18) are rewritten as

$$Z_{mn} = \Delta L_n \frac{jk}{4} (S^l + S^c + S^r) \quad (3-43)$$

where S^r , S^l and S^c represent the summations for the right, left and the center sections respectively and are given by

$$S^r = \cos \psi'_{p^+} \sqrt{\frac{2}{\pi k L}} e^{-j\left(k\Delta x - \frac{3\pi}{4}\right)} \left(S_0^r - \frac{1}{2} S_1^r \Delta x + \frac{3}{8} S_2^r \Delta x^2 - \frac{15}{48} \Delta x^3 + \dots \right) \quad (3-44)$$

$$S^l = -\cos \psi'_{p^-} \sqrt{\frac{2}{\pi k L}} e^{j\left(k\Delta x + \frac{3\pi}{4}\right)} \left(S_0^r + \frac{1}{2} S_1^r \Delta x + \frac{3}{8} S_2^r \Delta x^2 + \frac{15}{48} \Delta x^3 + \dots \right) \quad (3-45)$$

$$S^c = \sum_{p=-p_0}^{p_0} e^{jkL \sin \theta_i} H_1^{(2)}(kR_p) \cos \psi'_{p^+} \quad (3-46)$$

where S_v^r and S_v^l , $v=0,1,2,3,\dots$, are the universal summations given in (3-27) and (3-28) and $\cos \psi'_{p^+}$ is

$$\cos \psi'_{p^+} = \mathbf{n}' \cdot \mathbf{a}_{R_p} \approx \frac{p}{|p|} \frac{f'_s(x')}{\sqrt{1 + [f'_s(x')]^2}} \quad |p| > p_0 \quad (4-47)$$

$$\cos \psi'_{p^+} = \frac{(y-y') - (x-x'-pL)f'_s(x')}{\sqrt{(x-x'-pL)^2 + (y-y')^2} \sqrt{1 + [f'_s(x')]^2}} \quad |p| \leq p_0 \quad (4-48)$$

where $f'_s(x')$ is the first derivative of the surface slope.

CHAPTER IV.

ERROR AND COMPUTATIONAL-TIME ANALYSIS FOR PERIODIC-SURFACE MODEL

Introduction

In this chapter, the accuracy and computational efficiency of the periodic surface moment method models are analyzed. Appropriate choices for the various parameters in the models at different angles of incidence and surface conditions are determined.

Error Analysis for EFIE Periodic Surface Model

We again examine the reflection of a TM^z polarized uniform, plane wave from an infinite, perfectly conducting planar surface, as shown in Figure 5. The incident magnetic field is

$$\mathbf{H}^i(\rho) = \frac{E_0}{\eta_0} (\hat{a}_x \cos \theta_i - \hat{a}_y \sin \theta_i) e^{jk(x \cos \theta_i + y \sin \theta_i)} \quad (4-1)$$

where E_0 is the magnitude of the incident electric field and η_0 is the intrinsic impedance of the medium. The current density on the surface is known to be

$$\mathbf{J}_s = 2 \hat{n} \times \mathbf{H}^i = -\hat{a}_z \frac{2E_0}{\eta_0} \cos \theta_i \quad (4-2)$$

where \mathbf{J}_s is the current distribution on the surface, \hat{n} is the normal vector at the surface and θ_i is the incident angle.

This example is used to test accuracy of the EFIE PS model by comparing the current computed by the model with the closed form solution (4-2). The error in the current density for the problem is parameterized using the RMS relative error σ of the current across the reference section

$$\sigma = \frac{1}{\sqrt{N}} \sqrt{\sum_{i=1}^N \left| \frac{\tilde{J}_i - J_i}{J_i} \right|^2} \quad (4-3)$$

where N is the number of moment method segments on the reference section, \tilde{J}_i is calculated value of the current at the i th segment, and J_i is the exact value of the current at the i th segment. This definition of the error has the advantage of including the errors at all points on the surface, but weighting the larger errors more strongly than smaller errors. This is well suited to scattering calculations, where the errors may only be significant at the edge points, but gives a very poor predicted value for the scattered field.

Truncation Errors

Errors are introduced by the truncation of the infinite series in equations (3-8), (3-9) and (3-11), (3-12). Figure 7 shows the RMS relative error of the current obtained using the EFIE periodic surface model versus the incident angle. The length of the reference surface (and therefore the surface period) L was 10λ , the reference section was divided into 100 moment method segments, and M (the number of periodic sections used on each side of the reference section) was varied from 0 to 100,000. We immediately see that the errors in the calculated currents decrease as M increases. We also see that the errors are strongly dependent on the incident angle and are largest at large angles of incidence (near grazing). The main reason for this is that at the largest incident angles the magnitude of the current is quite small so the edge currents dominate and the relative error increases. At small incident angles only a few periodic sections are needed to greatly reduce the edge effects. However, in this specific problem, approximately 10,000 sections on each side of the reference section are required to reduce the RMS relative error to less than a few percent at all angles of incidence up to 89° .

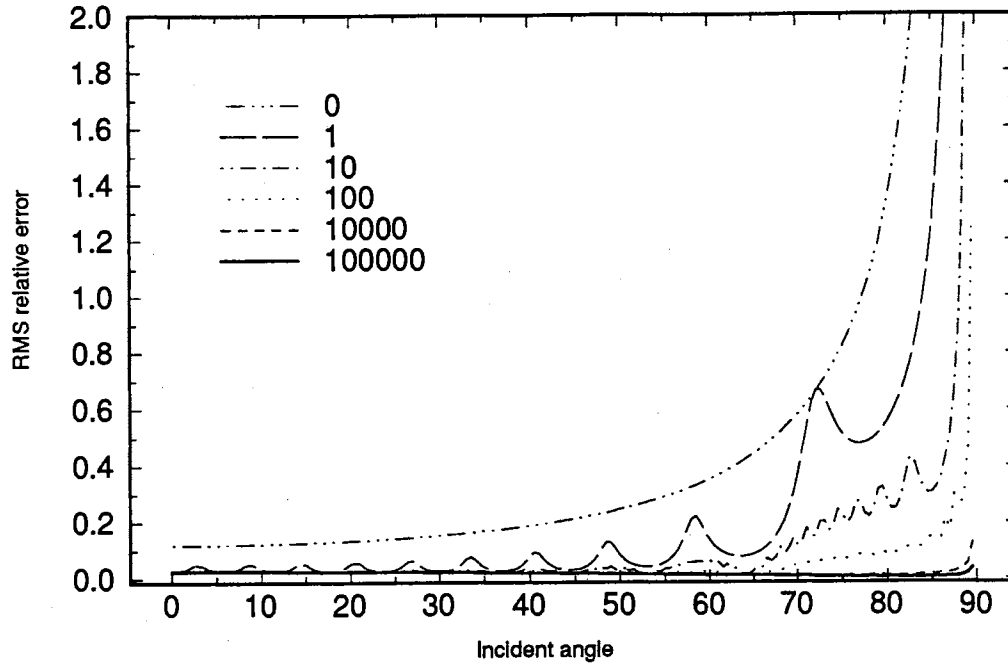


Figure 7. Comparison of RMS relative errors of the calculated current on an infinite flat plane using EFIE PS model with various periodic sections (M) vs. incident angle, TM polarization case.

Another truncation error results from the truncated Taylor expansion series in equation (3-21). The expansion argument is

$$\delta x = \frac{x - x'}{pL} \quad (4-4)$$

As will be shown, p must be greater than or equal to 2. Also, $|x - x'| < L$, so $\delta x < 1/2$. In this work, the Taylor expansion was truncated after 5 terms, so the error induced is of order $O(\delta x^6)$ and the maximum error (when $p=2$) is $O(1/64)$. Errors of this magnitude have no significant effect on the scattering calculation.

Discretization Errors

The pulse basis functions used in the moment method developed in the previous chapter were chosen to allow a simple evaluation of the interaction matrix elements. However, these are the crudest basis functions available, and lead to a greater discretization error than the more complicated basis functions. Thus, more basis functions are required to yield the same accuracy. Many works use 5-10 basis functions per radar wavelength along the surface, but this must be proven valid at high angles of incidence. Figure 8 shows the RMS relative error of the current on the infinite plane computed by EFIE PS model with various numbers of pulse basis functions per wavelength (N). M was fixed at 10,000 in all calculations. The figure shows that the error decreases as N increases at small incident angles (less than 70 degree) but almost no improvement is observed at large incidence. Even using the extended moment method, the major error at large

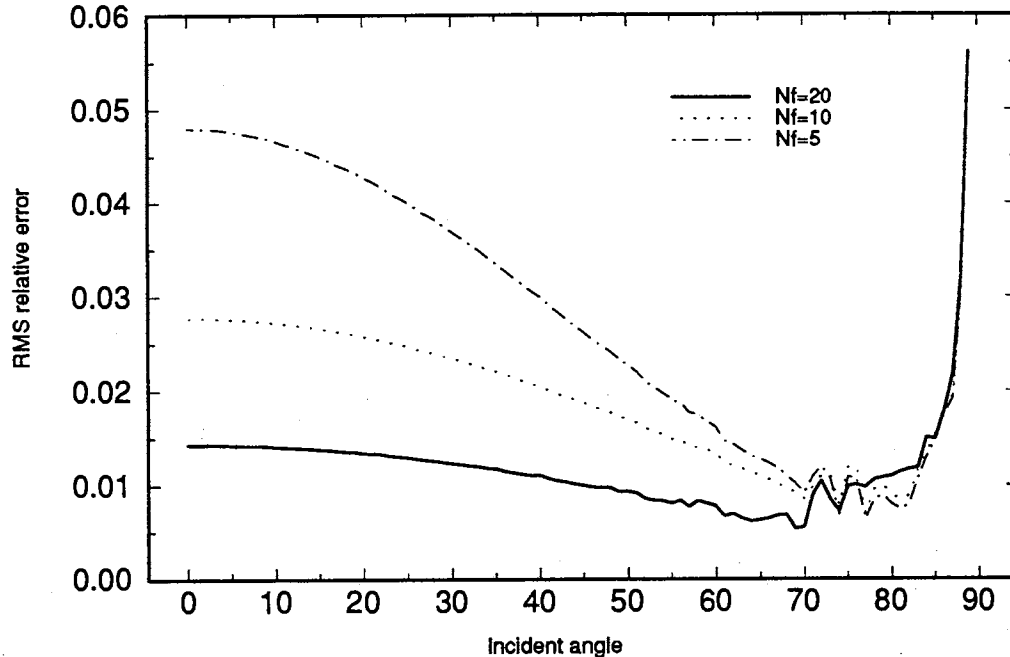


Figure 8. Discretization errors of the calculated current on an infinite flat plane using EFIE PS model for various basis functions per wavelength vs. incident angle, TM polarization.

incidence is caused by the edge effects. The figure also shows that when 5 basis functions are used the RMS relative error is near 5% at most incidence angles, so this is the minimum acceptable number. 20 basis functions per wavelength yields an RMS relative error less than 1.5% at small incident angles, but, as mentioned, very little improvement at the large incidence angles. In this work 10 basis functions per wavelength are used. This choice gives a good balance between accuracy and computational time.

Error with Period Length

The error in the calculated current will depend not only on the number of periodic sections used in the summation but also on the size L used to represent surface. Figure 9 shows the RMS relative error in the calculated currents when the surface is modeled with section periods of 2, 10, and 20λ . A fixed number of periods ($M=10,000$) and 10 moment segments per wavelength were used in all calculations. We see that the period affects the accuracy only at the largest incidence angles, and the model is more accurate with larger

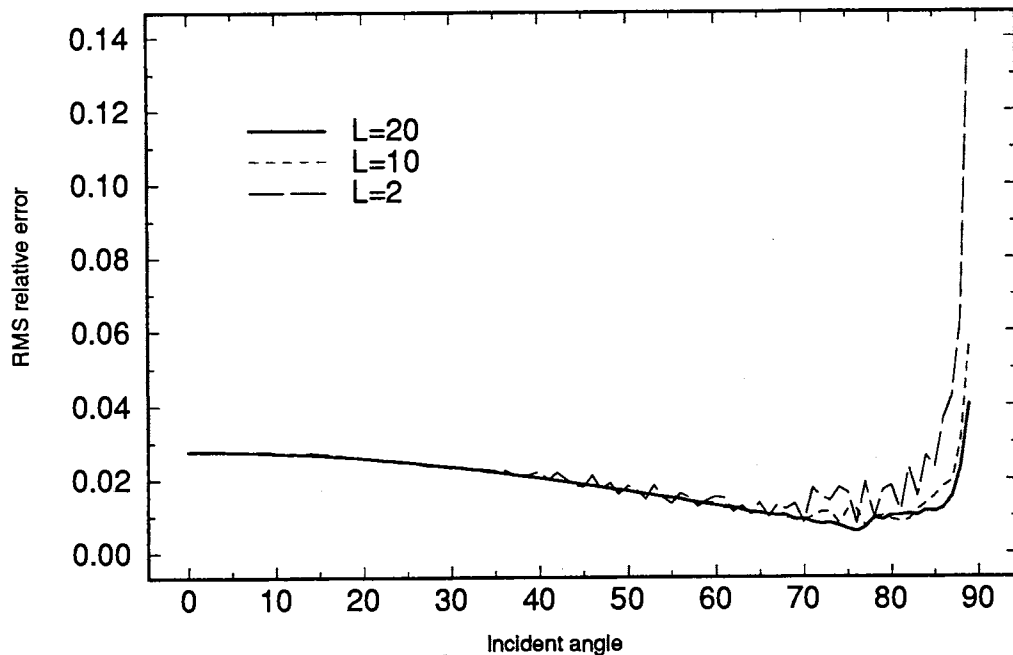


Figure 9. RMS relative errors of the calculated current on an infinite flat plane, using EFIE PS model at various period lengths L , sampling rate $10/\lambda$, TM

periods. This results simply because the value of M was fixed, so decreasing the period moves the edge closer to the reference section and the edge effects increase.

Error of Using Approximate Hankel Functions

Another error comes from the replacement of the Hankel function by its asymptotic form in equation (3-20):

$$H_0^{(2)}(kR_p) \approx \sqrt{\frac{2}{\pi k R_p}} e^{-jkR_p} \quad (4-5)$$

This expansion is valid when $kR_p \geq 10$. The minimum value of R_p is $(p-1)L$, so the first constraint on p is $p > 1 + \frac{10}{kL}$. Equation (4-5) is actually evaluated using the approximation (from equation (3-19)).

$$\begin{aligned} R_p &= \sqrt{[x - (x' + pL)]^2 + (y - y')^2} \\ &\approx x - (x' + pL) = \tilde{R}_p, \end{aligned} \quad (4-6)$$

The dominant error introduced by this approximation is in the phase kR_p . The error can be kept to below a maximum acceptable level of $\frac{\pi}{4}$ radians when the inequality

$$|R_p - \tilde{R}_p| \leq \frac{\lambda}{8} \quad \text{everywhere} \quad (4-7)$$

is met everywhere. The first error term in the expansion of R_p is

$$\frac{(y - y')^2}{2[x - (x' + pL)]} \quad (4-8)$$

so (4-8) becomes

$$\frac{(y - y')^2}{2[x - (x' + pL)]} \leq \frac{\lambda}{8} \quad (4-9)$$

The maximum value of $(x-x')$ is L , so the limit is

$$\frac{(y-y')^2}{(p-1)L} < \frac{\lambda}{4} \quad \text{everywhere} \quad (4-10)$$

Note that for the flat plate, this is always met since $(y-y')=0$ everywhere. For a random surface, the deterministic term $(y-y')^2$ is replaced by its expected value:

$$\frac{\sigma_y^2}{(p-1)L} < \frac{\lambda}{4}, \quad (4-11)$$

where σ_y is height variance of surface, thereby defining a second constraint on p .

Error Analysis for MFIE Periodic Surface Model

For the special case of scattering from an infinite planar surface, the MFIE reduces to the exact solution. Thus, no error evaluation can be performed with this example. Instead, another special periodic scattering problem, a uniform plane wave incident on an infinite surface that has a small magnitude sinusoidal oscillation, is used to indirectly analyze the error of the MFIE PS model. The surface is given by

$$y(x) = h \sin(Kx) \quad (4-12)$$

where h is the magnitude of the sinusoidal surface and K is the wave number of the surface. Figure 10 show the calculated current distribution using the PS models at an incident angle of 88° . Figure 10(a) is the current using EFIE PS model with various values of M , Figure 10(b) is the calculated current using the MFIE PS model with various values of M and Figure 10(c) is comparison of the currents calculated by the two models at the largest M . These figures show that the both models converge to the same current profile when M is increased despite their differences when $M = 0$. The EFIE PS model converges faster than the MFIE PS model as M increases and therefore is more suitable for use when available computer resources allow direct solution of the moment matrix

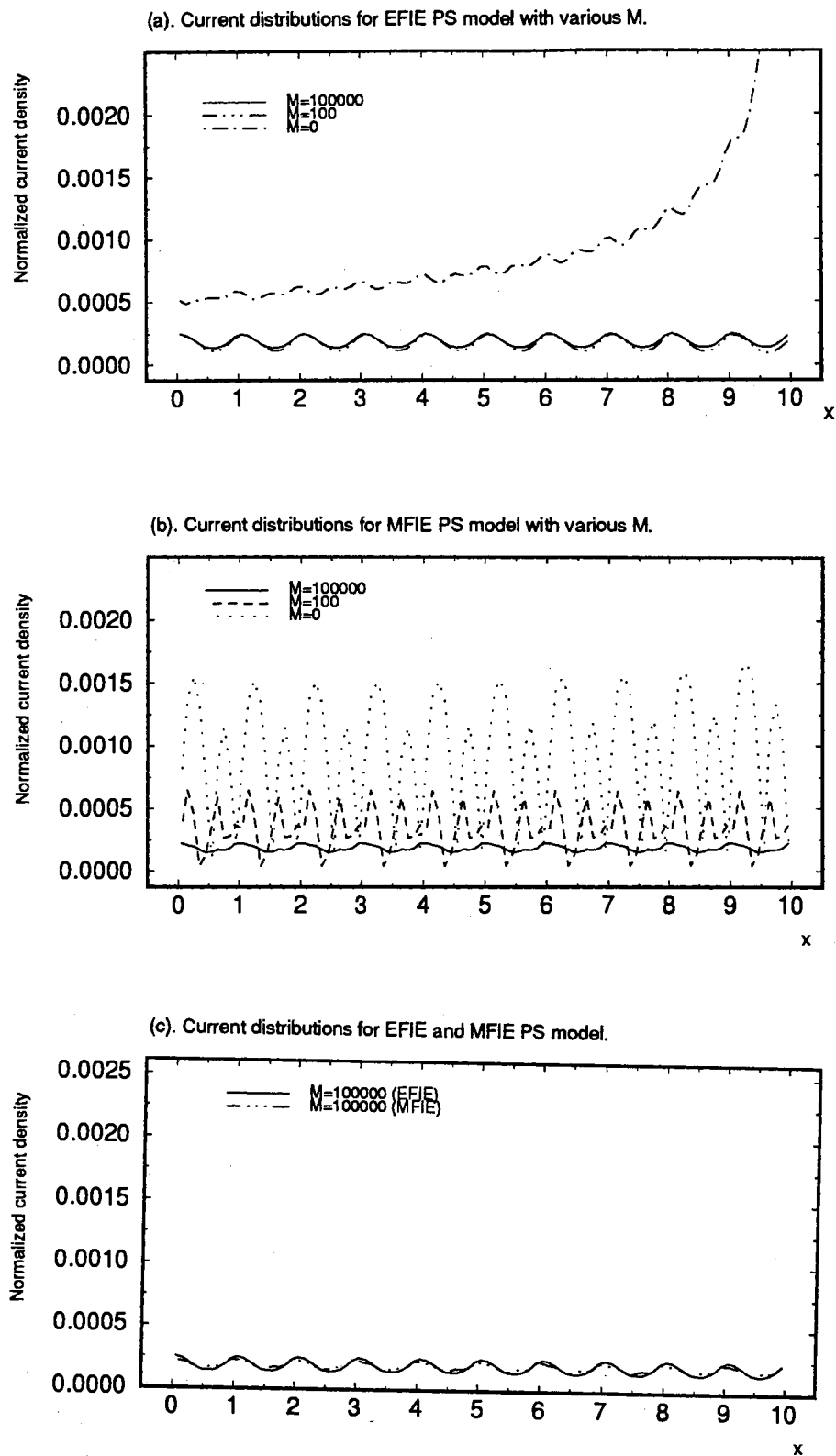


Figure 10. Calculated currents using EFIE and MFIE PS models for a sinusoidal surface, $K=k$, $h=0.1\lambda$, $\theta_i=88$ degree, TM polarization case.

equation. However, as mentioned before the MFIE implementation yields a well-conditioned matrix system that is more suitable for iterative solution.

Figure 11 shows RMS relative error of the current computed using the MFIE PS model versus the incident angle. The reference "exact" current was calculated using the EFIE PS model. The length of the reference surface (and therefore the surface period) L is 10λ , the magnitude $h=0.1\lambda$, the wave number K of the sinusoidal surface is equal to the radar wave number, and 100 moment segments (N) were used on the reference section. M was varied from 0 to 100,000. The dependence of the error on both angle of incidence and number of periodic sections is quite similar to that observed for the EFIE model. However, in this specific problem approximately 100,000 sections on each side of the reference section are required to reduce the RMS relative error to acceptable levels at large angles of incidence. Note that the reference is not exact, so the errors in the MFIE and EFIE PS models may reinforce each other.

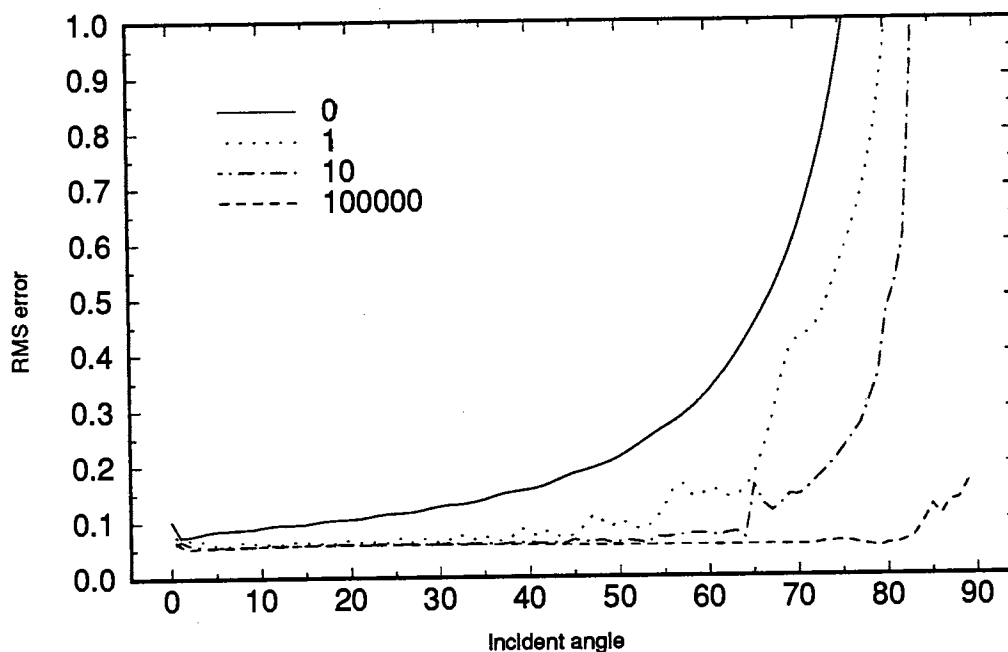


Figure 11. Comparison of RMS relative errors of the calculated current using MFIE PS model for various periodic sections vs. incident angle, sinusoidal surface, $K=k$, $h=0.1\lambda$, TM polarization case.

Computational-Time Analysis for PS Model

The time that the periodic surface model requires to evaluate the matrix elements can be divided into two parts, the exact evaluation of the Hankel function in equation (3-29) and the computation of the universal summations in equation (3-27) and (3-28). Note that equation (3-29) is order $O(N^2)$ times, where N is the number of moment segments on the reference section. Figure 12 shows the CPU time used by the EFIE PS model using both exact and the universal summation evaluation of the matrix elements. The scattering problem is the same as that used in error analysis, reflection of a TM^z wave from an infinite planar surface. The routine was implemented on an IBM RS6000 model 320 workstation. When the number of sections M is 2 or less, the universal summations are not used (p is always less than or equal to M), so the two techniques are identical. When $M > 2$, the CPU time increases linearly with the number of sections when exact evaluation is used. However, when the universal summations are used, the CPU time remains almost constant

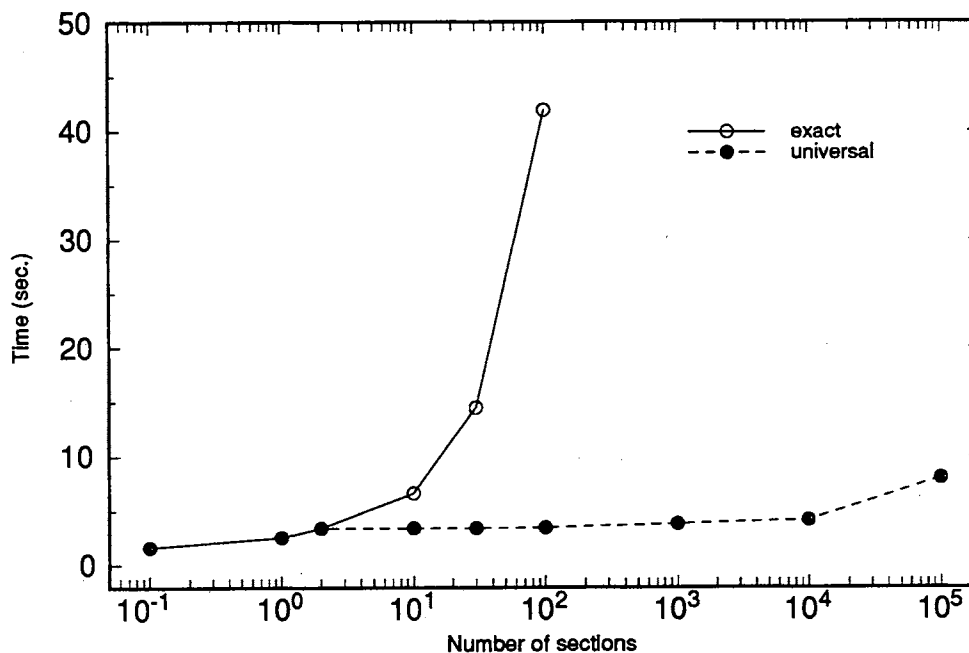


Figure 12. Comparison of computational time for the exact summation and the universal summation with various M . $N_m=100$ moment segments.

with M , indicating the majority of the time is spent performing the summations that are unique for the individual matrix elements (equation 3-29). (Note that all times include a fixed offset of about 1 second for the time required to solve the 100×100 matrix). This is true until $M > 10,000$, where the evaluation of the universal summations becomes significant and then dominates the time. When $M < 10,000$ the evaluation time using universal summations is only slightly greater than that for a standard moment method application to a single section. Even when $M = 100,000$, the evaluation is less than a factor of three greater. This result shows that the new moment method technique can be used to determine the scattering characteristics of certain types of periodic surfaces even at small grazing angles in a very reasonable calculation time.

CHAPTER V.
SCATTERING CALCULATIONS FROM
SIMPLE SURFACES

Introduction

In this chapter, the periodic-surface moment method is applied to some simple surfaces whose scattering characteristics are well known. The scattering characteristics from an infinite plane and several infinite sinusoidal modulated surfaces are calculated with the PS models at horizontal and vertical polarization at angles of incidence up to 89° . Their results are compared with the predictions of approximate scattering theories. The example surfaces and illumination conditions are chosen to be in regions where the approximate theories are known to be valid. The optimal number of surface periods that are included in the universal summations are evaluated in terms of computational efficiency and accuracy.

Calculation of Scattering Coefficient

TM^z (Horizontal) Polarization

The radar surface scattering coefficient is defined as the radar cross-section of a section of surface divided by its area (Ulaby et al., 1982). For surfaces that are rough in only one dimension this reduces to (for horizontal polarization)

$$\sigma^0 = \frac{2\pi R}{L_s} \frac{|E^s|^2}{|E^i|^2} \quad (5-1)$$

where L_s is the length of the scattering section, E^s is the scattered electric field, E^i is the incident electric field, and R is the distance from the source point to the observation point. The total electric field backscattered from the periodic surface is determined from (Harrington, 1968)

$$E^s = \eta k \frac{e^{-j(kR-3\pi/4)}}{\sqrt{8\pi k R}} \sum_{p=-M}^M \int_{pL}^{(p+1)L} J_z(x') e^{jkpL \sin \theta_i} e^{jk[(x'+pL) \sin \theta_s + y' \cos \theta_s]} \sqrt{1 + \left(\frac{dy'}{dx'}\right)^2} dx' \quad (5-2)$$

where L is length of the period, R is the distance from the source point on the section to the observation point ($\gg ML$), θ_s is the backscattering angle and $J_z(x')$ is the current on the reference surface period (here the relationship for the periodic currents given in (3-3) is used). For backscattering (monostatic scattering), the transmitter and receiver are at the same location, so $\theta_i = \theta_s$. Since the surface is periodic, (5-2) can be rewritten as

$$E^s = \eta k \frac{e^{-j(kR-3\pi/4)}}{\sqrt{8\pi k R}} \int_{L_0} J_z(x') e^{jk[x' \sin \theta_s + y' \cos \theta_s]} \sum_{p=-M}^M e^{j2kpL \sin \theta_i} \sqrt{1 + \left(\frac{dy'}{dx'}\right)^2} dx', \quad (5-3)$$

where L_0 indicates integration over the reference period only. The summation in (5-3) approaches zero as M is made large except when

$$m2\pi = 2kL \sin \theta_m \quad m=0, 1, 2, \dots \quad (5-4a)$$

or

$$m\lambda = 2L \sin \theta_m \quad m=0, 1, 2, \dots \quad (5-4b)$$

Thus, the backscattering coefficients can only be computed at the incident angle where (5-4b) is met. When this is true, the field scattered from any single surface period is independent of p and can be determined from the reference section current:

$$E^s = \eta k \frac{e^{-j(kR-3\pi/4)}}{\sqrt{8\pi k R}} \int_{L_0} J_z(x') e^{jk[x' \sin \theta_s + y' \cos \theta_s]} \sqrt{1 + \left(\frac{dy'}{dx'}\right)^2} dx' \quad (5-5)$$

The scattering coefficient (at angles where (5-4) is met) reduces to

$$\sigma^0 = \frac{2\pi R}{L} \frac{|E^s|^2}{|E^i|^2} \quad (5-6)$$

where L is the length of one period.

An additional constraint on the product $L \sin\theta_i$ is obtained by substituting (5-4a) into the universal summations in equation (3-27). For $v=0$, the summation reduces to

$$S_0^r = \sum_{p=p_0}^M e^{-jkpL} e^{-jpm\pi} \frac{1}{\sqrt{p}} \quad (5-7)$$

If L is a multiple of the radar wavelength, (5-7) reduces to

$$S_0^r = \sum_{p=p_0}^M (-1)^p \frac{1}{\sqrt{p}} \quad m \text{ odd} \quad (5-8a)$$

$$= \sum_{p=p_0}^M \frac{1}{\sqrt{p}} \quad m \text{ even} \quad (5-8b)$$

The summation in (5-8b) diverges. Therefore, only odd values of m should be chosen in (5-4). The final criterion therefore is

$$m\lambda = 2L \sin\theta_m \quad m=1,3,5,\dots \quad (5-9)$$

TE^z (Vertical) Polarization

The radar surface scattering coefficient for vertical polarization is defined as (Ulaby et al., 1982)

$$\sigma^0 = \frac{2\pi R}{L_s} \frac{|H^s|^2}{|H^i|^2} \quad (5-10)$$

where H^s is the scattered magnetic field and H^i is the incident magnetic field. Using a procedure similar to that for horizontal polarization, it can be shown that the

backscattering coefficients can be calculated only when equation (5-9) is met, and the scattered field from any period is determined entirely from the current on the reference period (Harrington, 1968):

$$H^s = k \frac{e^{-j(kR-3\pi/4)}}{\sqrt{8\pi k R}} \int_{L_0} J_c \cos \psi_n e^{jk[x' \sin \theta_s + y' \cos \theta_s]} \sqrt{1 + \left(\frac{dy'}{dx'}\right)^2} dx' \quad (5-11)$$

where

$$\begin{aligned} \cos \psi_n &= \hat{\mathbf{n}} \cdot \hat{\mathbf{R}} \\ &= \left(-\sin \theta_i + \frac{dy'}{dx'} \cos \theta_i \right) \frac{1}{\sqrt{1 + (dy'/dx')^2}} \end{aligned} \quad (5-12)$$

The backscattering coefficient for vertical polarization reduces to

$$\sigma^0 = \frac{2\pi R}{L} \frac{|H^s|^2}{|H^i|^2} \quad (5-13)$$

Scattering from Simple Surfaces at Horizontal Polarization

Scattering from an Infinite Plane

We first examine the reflection of a TM^z polarized uniform, plane wave from an infinite, perfectly conducting planar surface as was shown in Figure 5. Other than the specularly reflected field when $\theta_i=0$, there is no backscattered field. Any predicted backscattered field at non-normal incidence angles is entirely due to edge effects, so this example is used to determine if the model reduces the edge effects to values that are well below the expected scattering coefficients for actual surfaces. Figure 13 shows the backscattering coefficient calculated by the EFIE PS model at the incident angles that satisfy the condition in (5-9). The magnitude of the specular reflection at $\theta_i=0$ is accurately predicted even when only the reference section was used in the model ($M=0$).

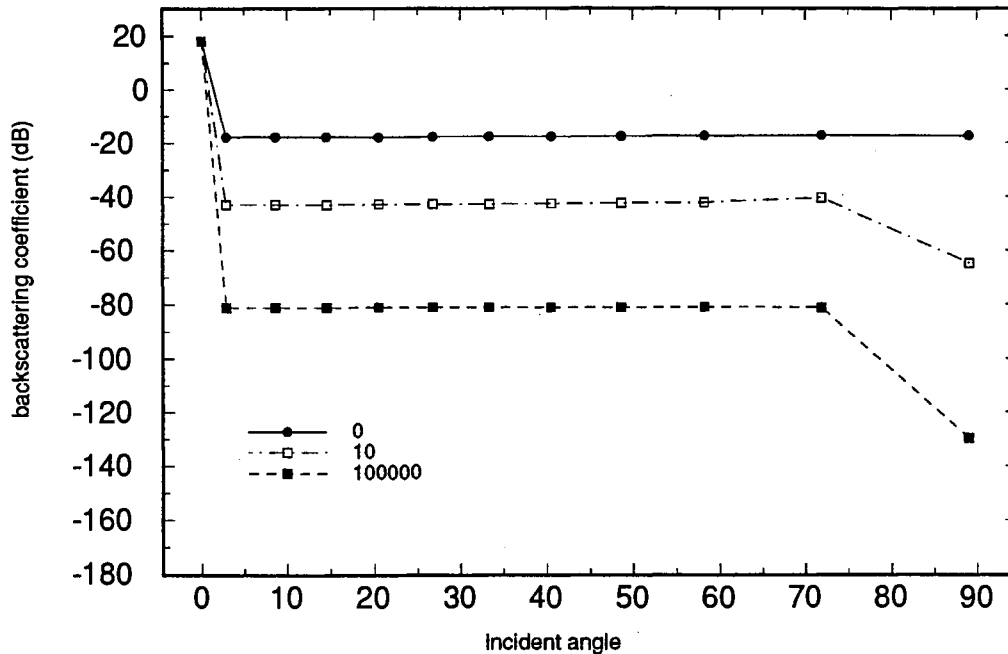


Figure 13. Backscattering coefficient calculated using the EFIE PS model for an infinite plane with various M .

However, the predicted scattering at other angles is quite high (-17 dB). This is much greater than the actual scattering coefficients experimentally measured from actual sea surfaces at small grazing angles (Guinard and Daley, 1970). Thus, the edge effects using this implementation would overwhelm the actual scattered field. Increasing the number of sections lowers the off-normal scattering coefficients until, when $M=100,000$, they are less than -80dB at all angles. This is sufficiently below the minimum backscattering coefficients of -50dB experimentally measured by Guinard and Daley at TM^z polarization.

Scattering from a Simple Sinusoidal Surface

Another special case where the backscattered field can be accurately predicted analytically is a uniform plane wave incident on an infinite surface that has a small magnitude sinusoidal oscillation. The surface displacement is given by

$$y(x) = h \sin(Kx) \quad (5-14)$$

where h is amplitude of the sinusoidal surface in wavelengths and K is wave number of the sinusoidal wave surface. If h is much smaller than the radar wavelength, the backscattered field can be accurately predicted by the small-perturbation (Bragg scattering) theory (Rice, 1951). Other than the specular reflection, the peak backscattered field occurs at the angle of incidence where the "Bragg-resonant" condition is satisfied (Ulaby et al., 1982):

$$|K| = 2k \sin \theta_B \quad (5-15)$$

where k is the wave number of the radar signal and θ_B is the Bragg-resonant angle of the incidence.

Figure 14 shows the backscattering coefficient calculated using the EFIE PS model. The surface amplitude h was 0.1λ and $K=1.1$, giving a Bragg-resonance angle of 33.4° .

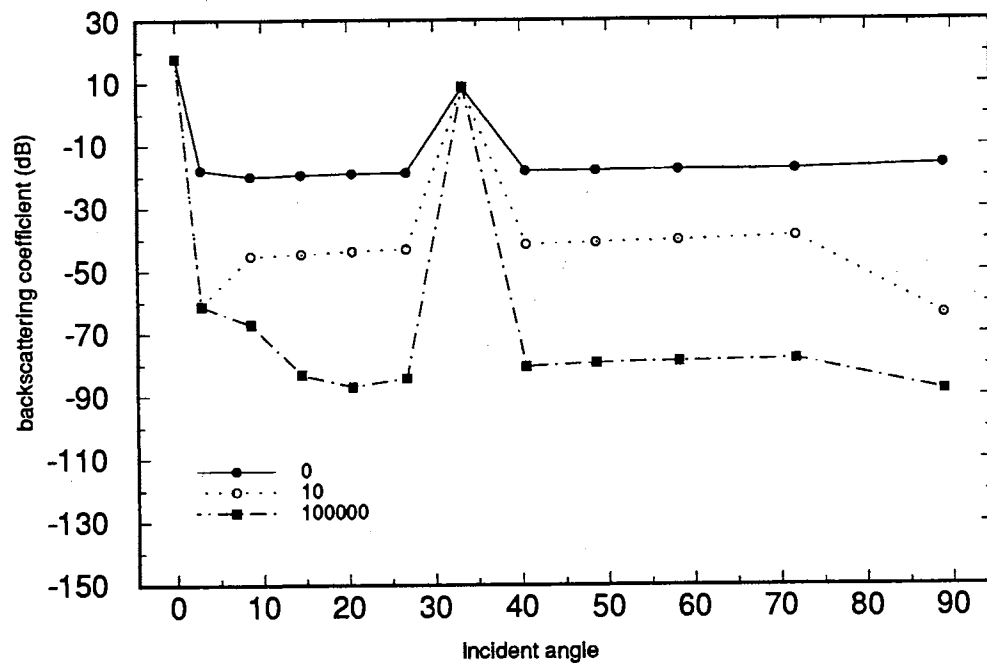


Figure 14. Backscattering coefficient calculated using the EFIE PS models for an infinite sinusoidal surface ($h=0.1\lambda$, $K=1.1k$) for various values of M .

The backscattering coefficient at the Bragg angle is accurately predicted independent of the number of sections used in the model. Again, using $M=100,000$ reduces the predicted scattering values at angles away from the Bragg angle and non-normal incidence to values well below that observed experimentally.

Figure 15 shows the backscattering coefficient calculated using the MFIE PS model for the same sinusoidal surface. For comparison, the scattering calculated using the EFIE with $M=100,000$ is also plotted in the same figure. The performance of the MFIE model is similar to that of the EFIE model when 100,000 sections are used. However, the EFIE model shows somewhat lower scattering coefficients at angles away from the Bragg angle and when fewer sections are used. Because of its inherent higher accuracy, the EFIE moment-method implementation is used for TM^z scattering for the remainder of this work.

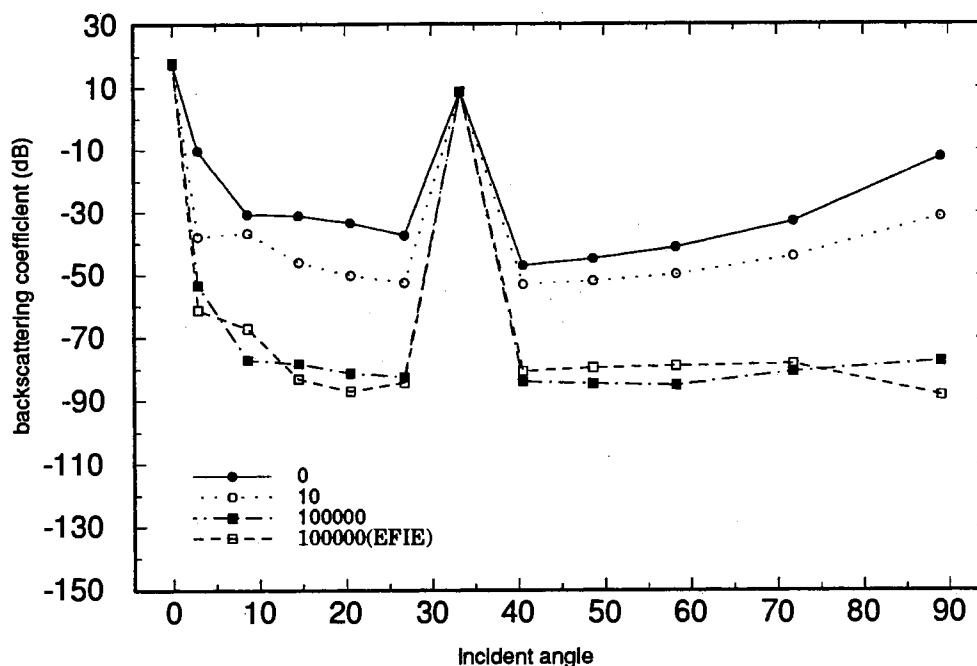


Figure 15. Backscattering coefficient calculated using the MFIE and EFIE PS models for an infinite sinusoidal surface ($h=0.1\lambda$, $K=1.1k$) for various values of

Scattering from Simple Surfaces at Vertical Polarization

The MFIE PS model for scattering at vertical (TE^z) polarization was also applied to sinusoidal surfaces. Figure 16 shows the calculated scattering from a sinusoidal surface with an amplitude of $h=0.1\lambda$ and a surface wavelength of $K=1.1k$. As with horizontal polarization, the magnitudes of the specular reflection at $\theta_i=0^\circ$ and the Bragg-resonant scattering at $\theta_i=33.4^\circ$ is accurately predicted independent of the number of periodic sections M used in the model. However, the edge effects at other incident angles (appearing as non-zero backscatter) depends strongly on M . When $M=100,000$, the off-Bragg scattering coefficients are -40dB at near normal incidence, -50dB at near grazing, and better than -70dB at angles in between. This is sufficiently below the corresponding backscattering coefficients from -20dB at near normal incidence to -40dB at near grazing incidence experimentally measured by Guinard and Daley (1970) for the actual ocean surface.

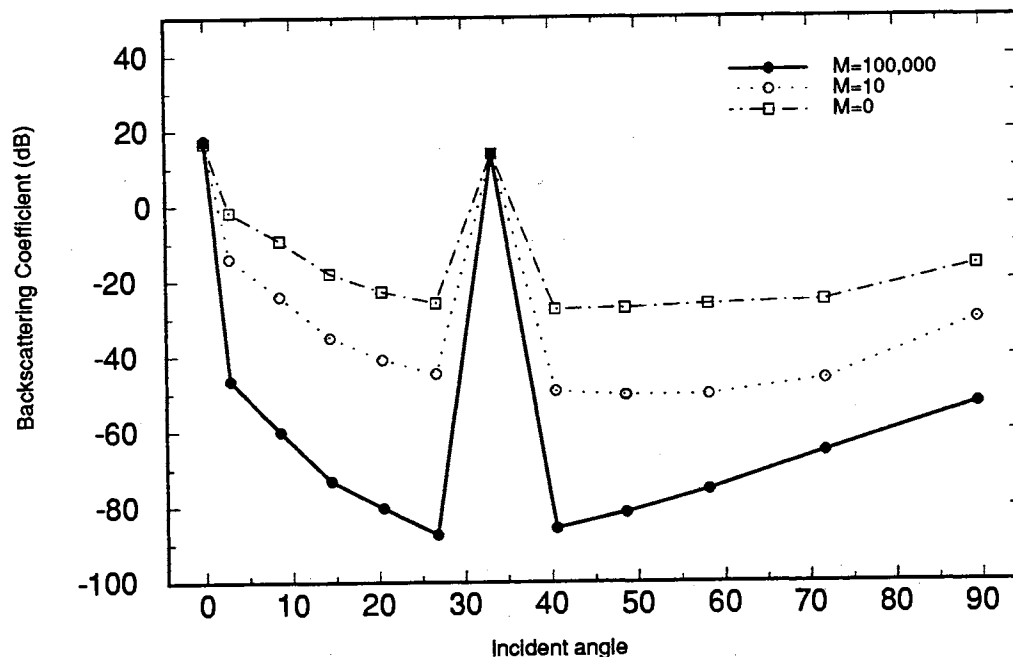


Figure 16. Backscattering coefficient (vertical polarization) for the PS model with various M from an infinite sinusoidal surface ($L=10$ unit, $h=0.1\lambda$, $K=1.1k$, $p_0=2$).

CHAPTER VI.

ROUGH-SURFACE SCATTERING CALCULATIONS

Introduction

In this chapter, the periodic surface moment method (PS model) is applied to various statistically differing types of rough surfaces. The calculated scattering is compared to the predictions of theoretical scattering models (small-perturbation method and Kirchhoff approximation) as well as with the scattering predicted using the traditional moment method with a tapered illumination weighting function. The scattering from surfaces whose power spectral density is described by a Gaussian envelope is first examined. While this type of surface is not found in nature, it is a simple single-scale surface whose scattering characteristics at moderate incident angles are well understood, allowing the numerical method to be tested. The scattering from a much more realistic power-law spectrum surface is then examined, and the validity of the two-scale description of this type of surface is investigated.

Traditional Scattering Models and Techniques

The Kirchhoff Scattering Model

The basic assumption of the Kirchhoff scattering (KS) model is that the current induced on the surface of the scatterer by the incident electromagnetic wave can be approximated by treating a local region of the surface as an inclined plane. The surface current is determined from the reflection of a plane wave from an infinite planar surface defined by the local slope of the actual surface. Here, the method of Chen and Fung (1988) is used to calculate the scattering predicted by the Kirchhoff approximation. The surface current is determined using the local tangent-plane approximation, and the

currents are then reradiated using equation (5-5) and (5-8). We first consider a uniform TM^z plane wave given by (2-6) incident on a one-dimensional rough surface (horizontal polarization). At an arbitrary point, the unit vector normal to the surface is given by

$$\hat{\mathbf{n}} = \frac{1}{\sqrt{1 + (dy/dx)^2}} \left(-\hat{\mathbf{a}}_x \frac{dy}{dx} + \hat{\mathbf{a}}_y \right) \quad (6-1)$$

where $\frac{dy}{dx}$ is the surface slope. The Kirchhoff current at an arbitrary point is

$$\begin{aligned} \mathbf{J} &= 2 \mathbf{n} \times \mathbf{H}^i \\ &= \hat{\mathbf{a}}_z 2H_0 \frac{1}{\sqrt{1 + (dy/dx)^2}} \left(\frac{dy}{dx} \cos \theta_i - \sin \theta_i \right) e^{jk_0(x \sin \theta_i + y \cos \theta_i)} \end{aligned} \quad (6-2)$$

Substituting (6-2) into (5-5), the far-zone backscattered field from one periodic section is

$$E^s = 2E_0 k \frac{e^{-j(kR - 3\pi/4)}}{\sqrt{8\pi kR}} \int_{L_0} \left(\frac{dy}{dx} \cos \theta_i - \sin \theta_i \right) e^{j2k[x \sin \theta_s + y \cos \theta_s]} dx \quad (6-3)$$

where $E_0 = H_0 \eta$ is the magnitude of the incident electric field. We now consider a TE^z (vertical polarization) wave described by (3-7). The surface current density is

$$\begin{aligned} \mathbf{J} &= 2 \hat{\mathbf{n}} \times \mathbf{H}^i \\ &= \frac{2H_0}{\sqrt{1 + (dy/dx)^2}} \left(\hat{\mathbf{a}}_x + \hat{\mathbf{a}}_y \frac{dy}{dx} \right) e^{jk_0(x \sin \theta_i + y \cos \theta_i)} \end{aligned} \quad (6-4)$$

Substituting (6-4) into (5-8) yields

$$H^s = 2H_0 k \frac{e^{-j(kR - 3\pi/4)}}{\sqrt{8\pi kR}} \int_{L_0} \left(\frac{dy}{dx} \cos \theta_i - \sin \theta_i \right) e^{j2k[x \sin \theta_s + y \cos \theta_s]} dx \quad (6-5)$$

Comparing (6-5) with (6-3), we see that the ratio of the scattered field to incident field at horizontal polarization (H^s/H_0) is identical to the scattered field to the incident field

ratio at vertical polarization (E^s/E_0). Thus, the Kirchhoff model predicts no dependence on polarization for backscattering from a perfectly conducting surface. The mathematical restrictions for the validity of this model has been stated as (Ulaby et al., 1982; Bechmann and Spizzichino, 1963)

$$2k\Gamma \cos^3\theta_L \gg 1 \quad (6-6)$$

and

$$kl > 6 \quad (6-7)$$

where Γ is the surface radius-of-curvature at any point, l is the correlation length and θ_L is the local angle of incidence. Because of the $\cos\theta_L$ dependence in (6-6), this method is typically only valid at small incidence angles.

Small Perturbation Model

The small perturbation model (SPM) is another widely used model in practical applications (Rice, 1951). For this model, the induced surface current and scattered field are solved for a smooth surface. The fields are then perturbed to account for the small-scale roughness. The primary scattering mechanism predicted by SPM is Bragg-resonant scattering. The backscattering coefficients of the small perturbation model for a one-dimensional random surface are given by (Chen and Fung, 1988)

$$\sigma_{hh}^0 = 8\pi k^3 \cos^4\theta W(2k \sin\theta) \quad (6-8)$$

$$\sigma_{vv}^0 = 8\pi k^3 (1 + \sin^2\theta)^2 W(2k \sin\theta) \quad (6-9)$$

where k is radar wave number, θ is the incident angle, $W(K)$ is the surface power spectral density, and hh and vv represent horizontal (TM^z) and vertical (TE^z) polarization respectively. Note that $K=2k \sin\theta$ is the Bragg-resonant surface wave number.

At moderate incident angles ($20^\circ < \theta_i < 70^\circ$) Chen and Fung (1988) showed this model accurately predicted the backscatter when

$$k\sigma < 0.3 \quad (6-10)$$

and

$$\frac{\sqrt{2} \sigma}{l} < 0.3 \quad (6-11)$$

where σ is the standard deviation of the surface roughness and l is the correlation length. These conditions require that both the surface height and the surface slope are small electromagnetically. Also SPM does not predict coherent (specular) reflection, so it is not valid at small incident angles.

Moment Method with Illumination Weighting Function

Many different illumination weighting functions have been used to reduce the edge effects in moment method calculations of scattering from rough surfaces. (Jordan and Lang, 1979, Fung and Chen, 1985; Thorsos, 1988). In this work, the weighting function given by Fung and Chen, (1985) was used:

$$G(x_m) = \exp \left[-\frac{(x_m - x_0)^2 \cos \theta_i}{g^2} \right] \quad (6-12)$$

where x_0 is the center of a surface and g is a constant used to control the width of the tapered beam. The width factor $g=L/5.6$, where L is the total length of the surface modeled, was used. The effective illuminated width L_{eff} of the surface using this weighting function is

$$L_{eff} = \int_{-\infty}^{\infty} \exp \left(-\frac{2x^2 \cos^2 \theta}{g^2} \right) dx = \frac{g\sqrt{\pi/2}}{\cos \theta} \quad (6-13)$$

Scattering Calculations

The power backscattered from a randomly-rough surface follows an exponential distribution (Ulaby et al., 1982). Therefore, the expected backscattering coefficient from a rough surface is obtained by calculating the scattering from a number of independent surfaces and averaging. The noncoherent backscattering coefficient estimated from these surfaces is (Fung and Chen, 1985)

$$\sigma^0(\theta) = \frac{2\pi R}{N_s L_{eff}} \left[\sum_{j=1}^{N_s} |A_j^s|^2 - \frac{1}{N_s} \left| \sum_{j=1}^{N_s} A_j^s \right|^2 \right] \quad (6-14)$$

where N_s is the number of independent surfaces, R is the distance between the far zone observation point and the source point, and A_j^s is the normalized scattered field for the j th surface (E_j^s/E_0^i for horizontal polarization or H_j^s/H_0^i for vertical polarization).

The relative standard deviation of the estimated scattering coefficient is given by (Ulaby et al., 1982)

$$S.D. = \frac{1}{\sqrt{N_s}} \quad (6-15)$$

Here, $N_s=120$ was used when the scattering from a surface having a Gaussian power spectrum was calculated and $N_s=40$ was used when power-law spectrum surfaces were examined, yielding RMS errors of 9.2% (± 0.4 dB) and 16% (± 0.64 dB), respectively. The exact length L of the surfaces in the moment method calculations was varied so that equation (5-9) was met in the periodic-surface calculations. L was chosen to be approximately 10 radar wavelengths for Gaussian surfaces and least one cycle length of the longest surface wave for power-law surface. Per the error analyses in Chapter IV, 10 or more moment segments were used per radar wavelength along the surface in all but one case, thereby limiting the discretization errors in the calculated current to about 3%. In the other case, seven segments were used per wavelength so that the moment system would

not exceed the memory of the computer system used. In this case, the discretization error increased to approximately 5%. Similarly, the universal summations in equations (3-25) and (3-26) were carried out to 100,000 terms ($M=100,000$), allowing the PS moment method to be applied at angles of incidence up to 89° . The number of periods over which the Hankel function in the infinite series must be evaluated exactly (defined by p_0 in equation (3-29)) was determined automatically from equation (4-11). For all surfaces, $p_0 = 2$ was sufficient.

Generation of Random Surfaces

The sample random surfaces used in the scattering calculations were generated using the spectral technique summarized here. The autocorrelation of a random surface is (Sklar, 1988)

$$R(\tau) = E[y(x)y(x - \tau)] \quad (6-16)$$

where $y(x)$ is the profile of a sample surface and $E[]$ is the expected value operator. The power spectral density $W(K)$ of the surface is the Fourier transform of the autocorrelation function

$$\begin{aligned} W(K) &= \frac{1}{2\pi} \int_{-\infty}^{\infty} R(\tau)e^{-jK\tau} d\tau \\ &= F[R(\tau)] \\ &= E\{F[y(x)y(x - \tau)]\} \\ &= E\{|Y(K)|^2\} \end{aligned} \quad (6-17)$$

where K is the surface wave number, $F[]$ indicates the Fourier transform, and $Y(K)$ is the Fourier transform of $y(x)$. $Y(K)$ is often referred to as the amplitude spectrum of a single sample surface, while $W(K)$ is the power spectral density of the random process which defines the surface statistics. Equation (6-17) is satisfied when

$$Y(K) = N(K)\sqrt{W(K)} \quad (6-18)$$

where $N(K)$ is the Fourier transform of a real, white noise process $n(x)$. This is shown by substituting (6-18) into (6-17):

$$\begin{aligned} W(K) &= E\left\{\left[N(K)\sqrt{W(K)}\right]^2\right\} \\ &= E[N^2(K)]E[W(K)] \\ &= W(K) \end{aligned} \quad (6-19)$$

Thus, a random surface with an autocorrelation function $R(\tau)$ and power spectrum $W(K)$ is obtained by taking the inverse Fourier transform of the sample surface amplitude spectrum $Y(K)$:

$$y(x) = F^{-1}[Y(K)] = F^{-1}\left[N(K)\sqrt{W(K)}\right] \quad (6-20)$$

Note that when the inverse Fourier transform in equation (6-20) is evaluated numerically using a discrete (or fast) Fourier transform the resulting surface is naturally periodic, ideally suited for use with the periodic-surface scattering techniques.

The correlation length of the surface is defined by (Shanmugan and Breipohl, 1988)

$$l = \frac{1}{\sqrt{\pi}} \frac{\int_{-\infty}^{\infty} R(\tau) d\tau}{R(0)} \quad (6-21)$$

where $R(\tau)$ is the autocorrelation function of a surface.

Scattering from Gaussian Surface

In this section, the scattering from surfaces whose autocorrelations and power spectral densities are described by zero-mean Gaussian functions is examined. Although this does not produce surfaces that approximate those found in nature, they do provide well-understood surfaces under which the periodic-surface moment method can be tested (Fung and Chen, 1985). The autocorrelation function of this type of surface is

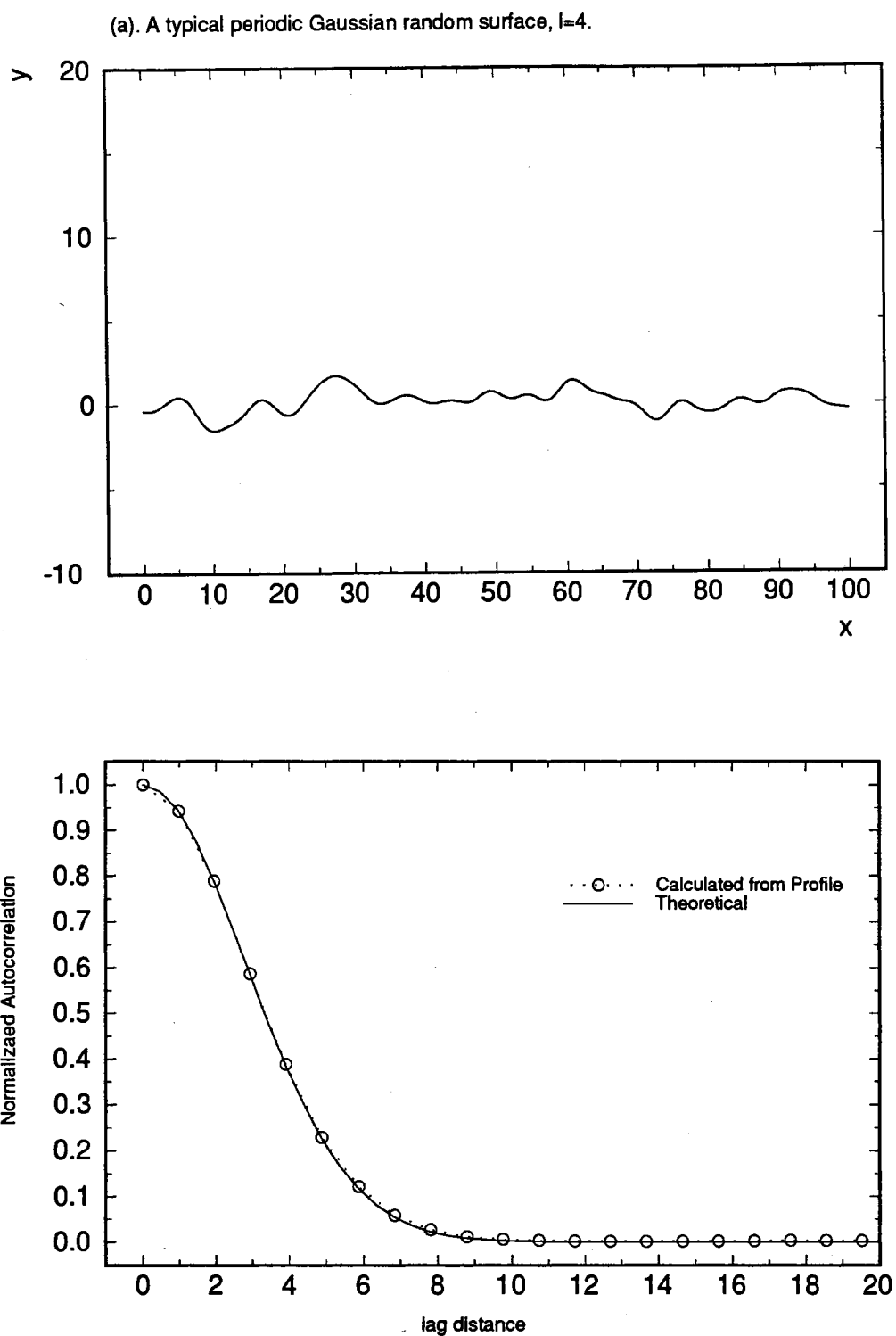


Figure 17. A typical Gaussian surface and its autocorrelation function. $l=4$ units, $\sigma=1$ unit.

$$R(\tau) = \sigma^2 \exp[-(\tau/l)^2] \quad (6-22)$$

where l is the surface correlation length defined by (6-21) and σ^2 is the variance of the surface displacement. The power spectral density is also Gaussian:

$$W(K) = \frac{\sigma^2 l}{2\sqrt{\pi}} \exp\left(-\frac{l^2 K^2}{4}\right) \quad (6-23)$$

Figure 17(a), shows a typical Gaussian surface with correlation length of 4 units and standard deviation of 1 unit, generated using the spectral technique. Figure 18(b) shows the autocorrelation estimated from 100 independently generated surfaces. Also shown is the theoretical autocorrelation plotted from equation (6-22). The calculated and theoretical autocorrelations show excellent agreement.

The scattering from Gaussian surfaces with two different statistical descriptions was calculated at three radar wavelengths. The correlation length was 4 units for both surfaces, and roughness standard deviations of 1.432 and 0.716 were used. The surface statistics and radar wavelengths used are identical to those used by Fung and Chen (1985), but the angle of incidence is extended to 89° here. The surface lengths used in the moment method at the different radar wavelengths and angles of incidence meet the conditions in eqn. (5-9), and are shown in Table-1.

Table 1. Surface lengths (unit) used in moment method computations for different incident radar wave lengths and various incident angles

| | | Angle of incidence (degrees) | | | | | | | | | |
|------------|-----|------------------------------|-------|-------|-------|-------|-------|-------|-------|-------|--------|
| | | 2.87 | 14.48 | 26.74 | 40.54 | 58.21 | 71.81 | 80 | 84 | 87 | 89 |
| Radar | 36 | 360 | 360 | 360 | 360 | 360 | 360 | 347.2 | 343.8 | 342.4 | 342.05 |
| wavelength | 9 | 90 | 90 | 90 | 90 | 90 | 90 | 86.82 | 85.97 | 85.62 | 85.51 |
| (units) | 4.5 | 45 | 45 | 45 | 45 | 45 | 45 | 43.41 | 42.99 | 42.81 | 42.76 |

Results

Figures 18(a)-(c) show the calculated backscattering coefficients at horizontal polarization from a Gaussian surface whose roughness standard deviation is 1.432 units at radar wavelengths of 36, 9, and 4.5 units. Shown are the predictions of the periodic-surface moment method (MMPS), the traditional moment method using a tapered illumination weighting function (MMTW), and the Kirchhoff approximation. At angles of incidence less than 60° , the results here are identical to those of Fung and Chen (1985). At small and moderate incident angles, the moment method calculations using both the periodic surface and the illumination weighting function are nearly identical for all surface roughnesses. However, MMTW gives much higher scattering values at angles greater than

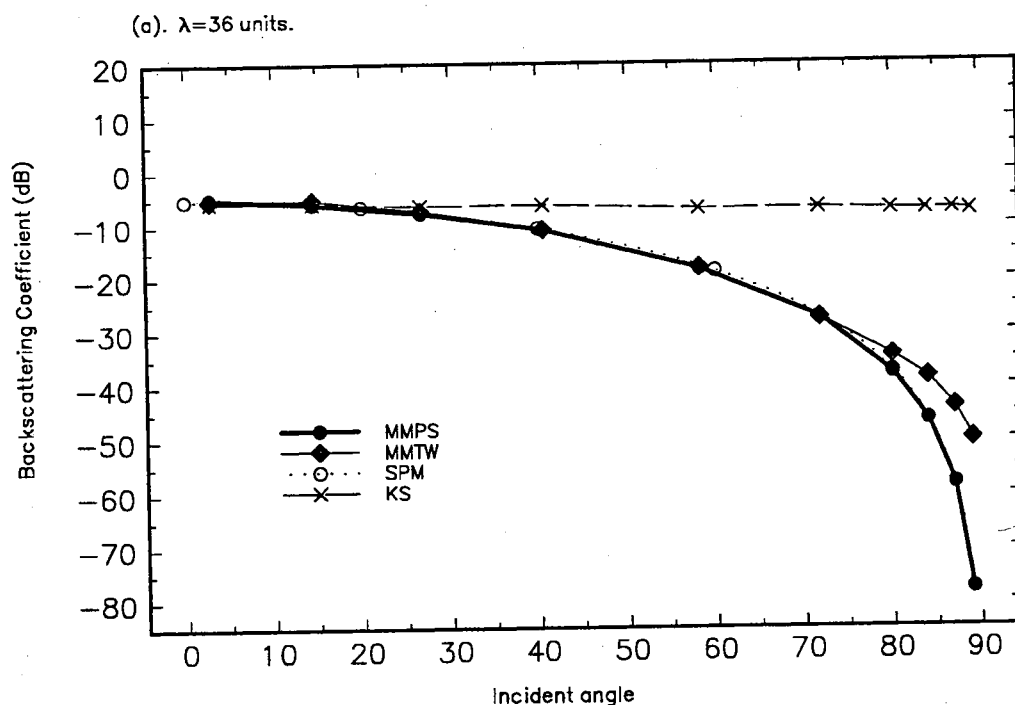


Figure 18. Backscattering coefficient of Gaussian surface, $\sigma=1.432$ units horizontal polarization.

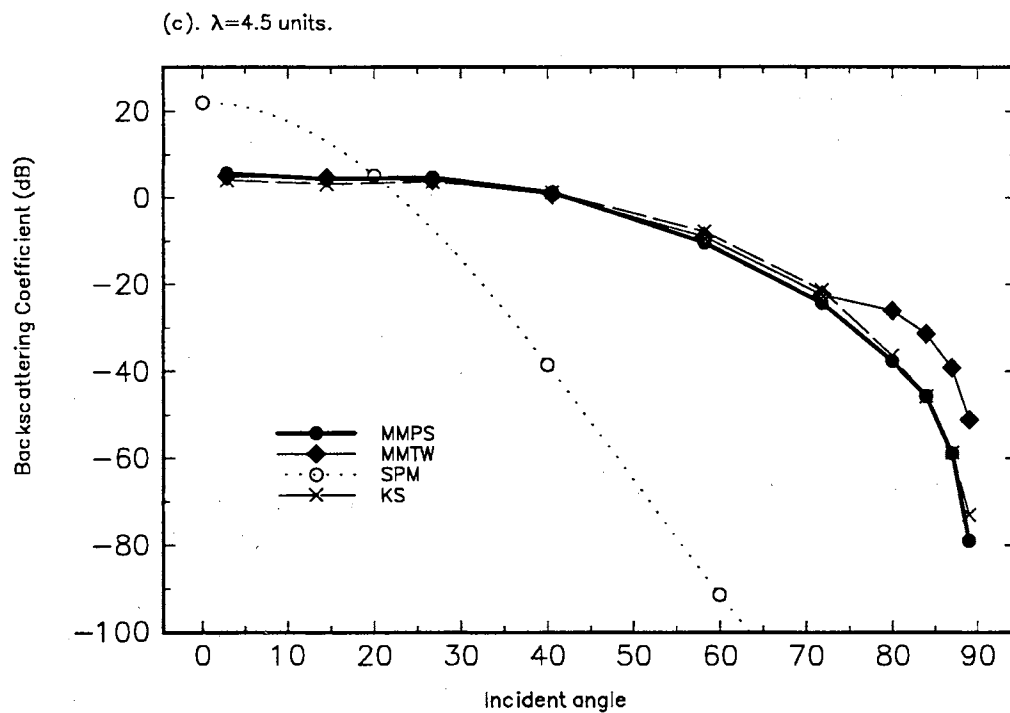
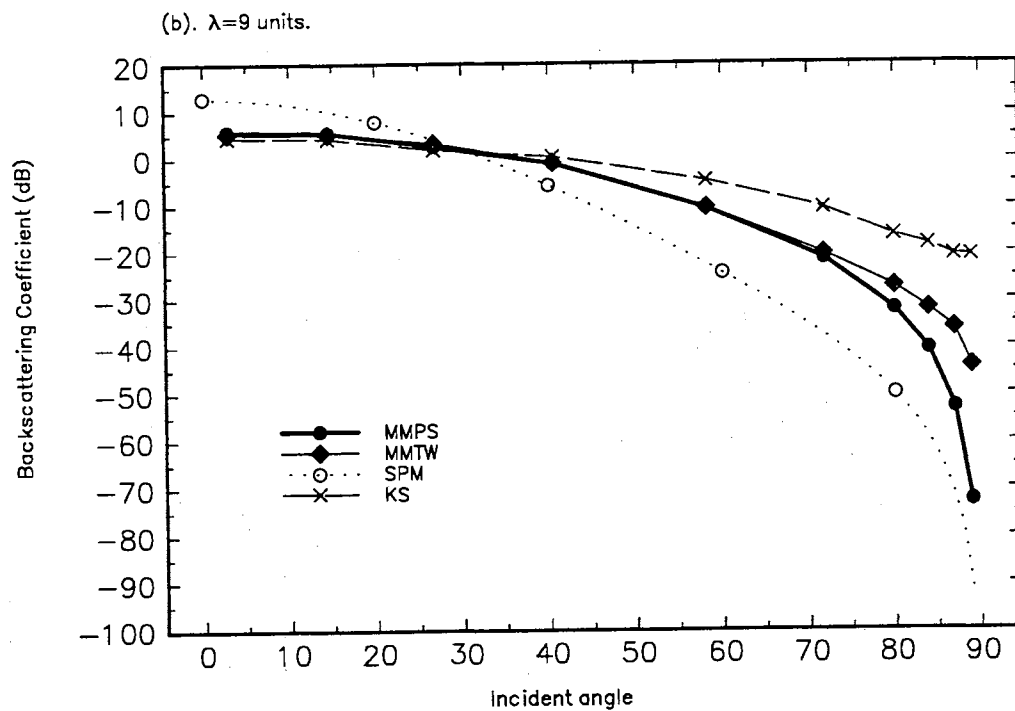


Figure 18(cont.). Backscattering coefficient of Gaussian surface, $\sigma=1.432$ units horizontal polarization.

70° at all radar wavelengths.

Figure 18(a) shows the backscattering coefficients calculated when the radar wavelength was 36 units. The values predicted theoretically using SPM agree with the calculations of MMPS to within 1dB at angles of incidence up to 89° (the largest modeled). The Kirchhoff approximation shows good agreement with the PS moment method at small incident angles ($\theta < 25^\circ$), but shows very poor agreement at larger angles.

Figure 18(b) shows the backscattering coefficients from the same surface as in Figure 18(a), but with the radar wavelength reduced to 9 units (the radar frequency is increased). At this wavelength, SPM does not agree with MMPS at any incident angle. The Kirchhoff approximation agrees with MMPS calculations when $\theta_i < 40^\circ$. Figure 18(c) shows the backscattering coefficients from the same surface when the radar wavelength was further reduced to 4.5 units. In this case, the Kirchhoff approximation agrees quite well with the MMPS calculations at all angles of incidence, while SPM does not agree well at any angle.

Figure 19 shows the scattering at vertical polarization from the same surface as in Figure 18. Again the periodic-surface and illumination-weighting-function moment calculations give nearly identical results at small and moderate incident angles, but the weighting function gives significantly higher values when $\theta_i > 80^\circ$. In part (a) of Figure 19, the radar wavelength was 36 units. At this wavelength, the MMPS numerical results agree with SPM predictions at angles of incidence up to 72°. However, at larger angles the MMPS coefficients drop rapidly with increasing angle while the SPM predictions continue to increase. At $\theta_i = 89^\circ$, SPM predicts backscatter that is 30dB higher than that calculated. The Kirchhoff approximation agrees with numerical predictions at angles less than about 20°.

The radar wavelength has been reduced to 9 units in part (b) of Figure 19. In this case, SPM does not agree with MMPS at any incident angle. The Kirchhoff approximation shows fairly good agreement with MMPS when $\theta_i < 60^\circ$, but rapidly diverges at larger angles. Again, the backscatter predicted by MMPS drops rapidly at large angles of incidence.

In Figure 19(c) the radar wavelength has been further reduced to 4.5 units. In this case, the Kirchhoff model agrees with the MMPS calculations out to 70 and rapidly drops at greater incidence. The SPM does not agree well at any angles.

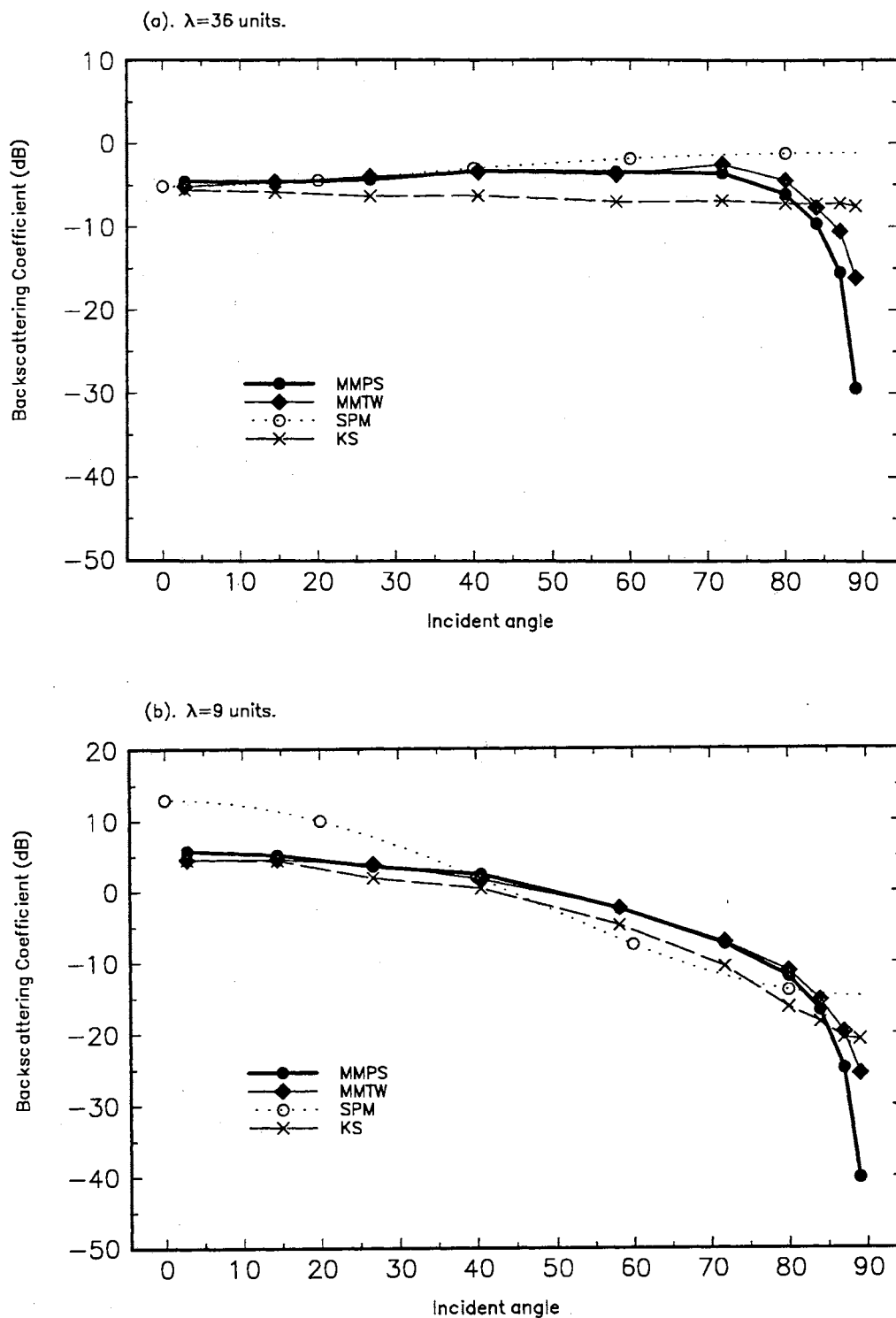


Figure 19. Backscattering coefficient of Gaussian surface, $\sigma=1.432$ units, vertical polarization.

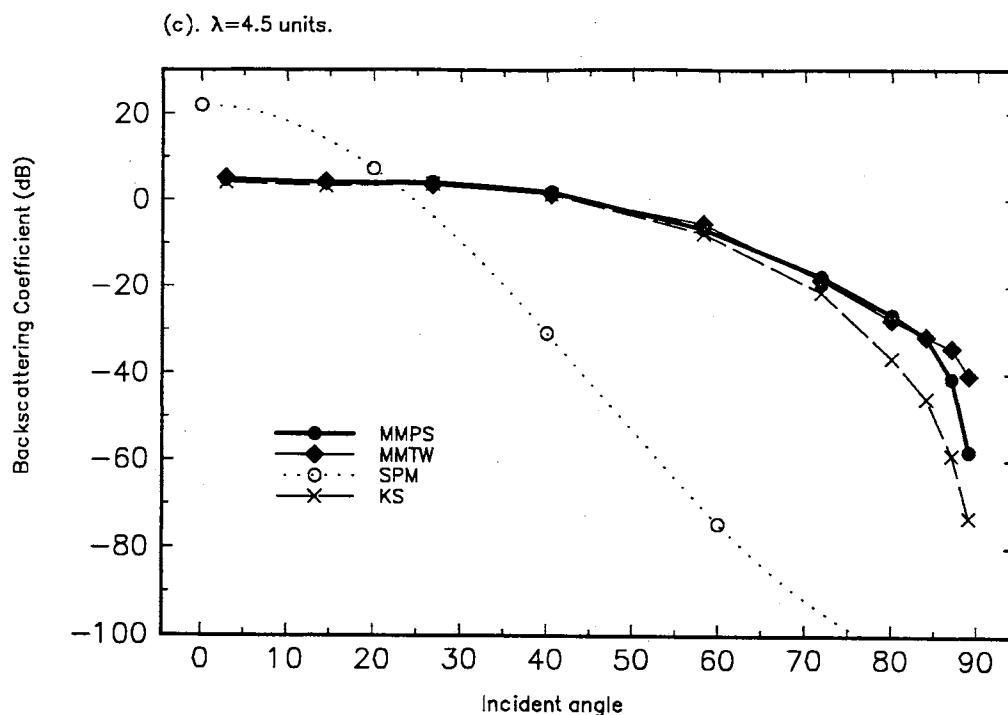


Figure 19(cont.). Backscattering coefficient of Gaussian surface, $\sigma=1.432$ units, vertical polarization.

The scattering calculations were also applied to a surface whose roughness was reduced by a factor of 2 (roughness standard deviation of 0.7163). The results are shown in Figures 20 and 21, for horizontal and vertical polarization, respectively. The dependence of the backscattering coefficient on angle of incidence predicted by the various theoretical and numerical techniques are quite similar to that obtained with the rougher surface. The primary difference is that the Kirchhoff approximation does not agree with MMPS numerical results as well at the smallest radar wavelength at large incidence angles for horizontal polarization.

Discussions

The calculations confirm that the periodic-surface moment method implementation overcomes the limitations of the traditional moment method (with an illumination weighting function) when calculating the scattering from random rough surfaces at large incidence angles. This is primarily demonstrated by the excellent agreement between SPM and the numerical results in Figure 18(a) and 20(a) and between the Kirchhoff approximation and the numerical results in Figure 18(c) and 20(c). Although the agreement between the theoretical models and the numerical results is not as good at large incidence at vertical polarization as at horizontal polarization, this is due to limitations in the scattering theories and not the numerical technique.

SPM has been previously shown to accurately model the scattering from Gaussian surfaces at angles of incidence less than 60° when the conditions of (6-10) and (6-11) are

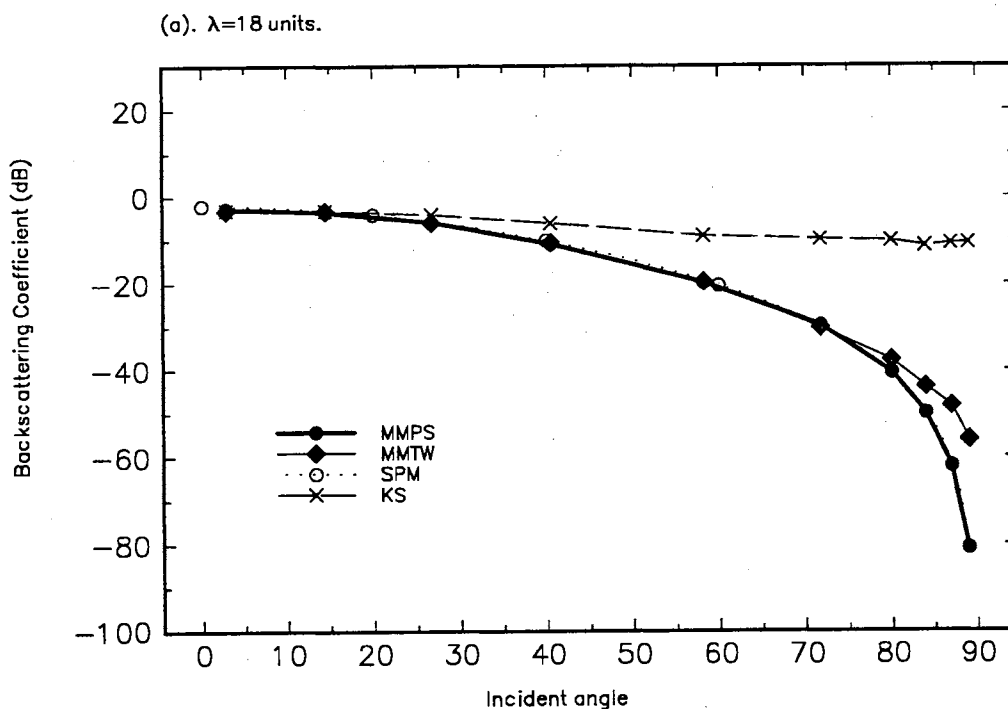


Figure 20. Backscattering coefficient of Gaussian surface, $\sigma=0.7163$ units, horizontal polarization.

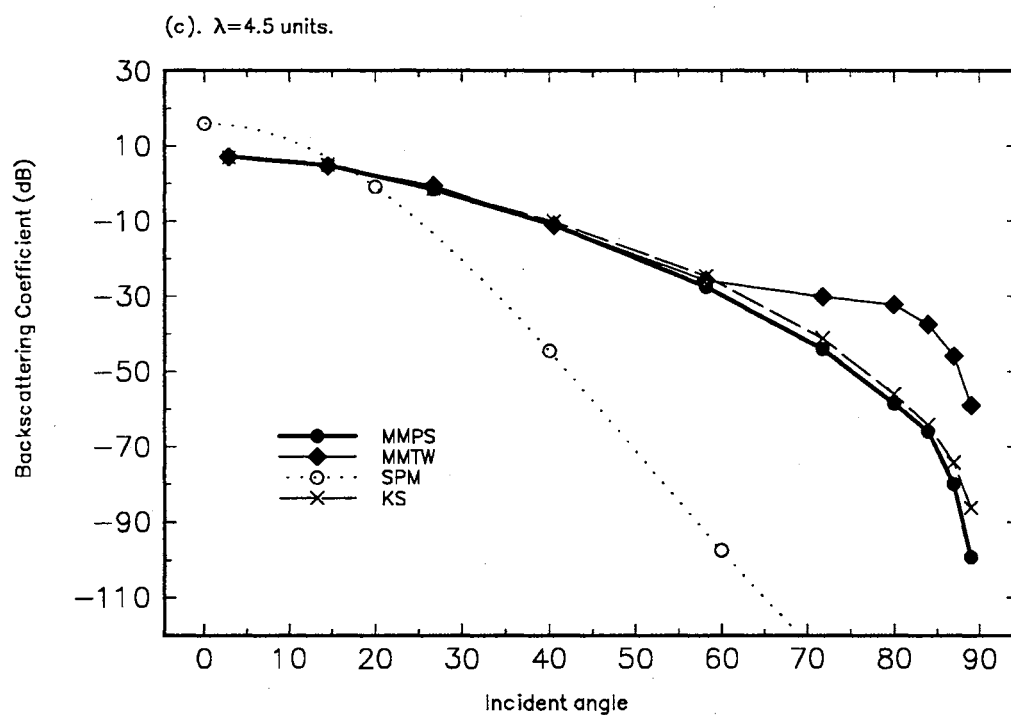
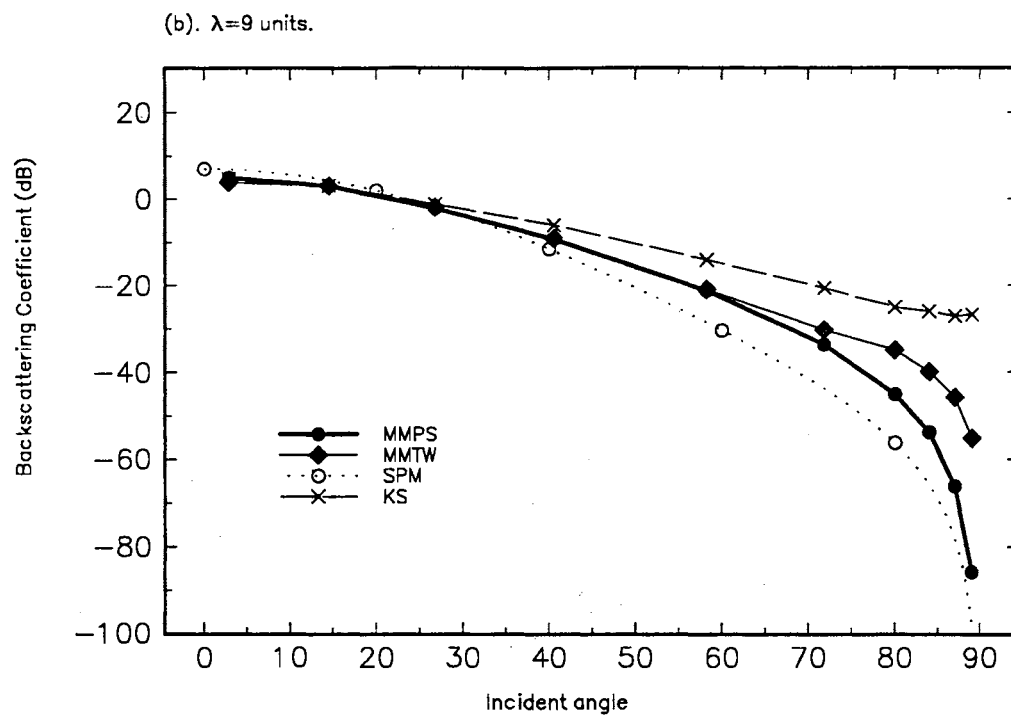


Figure 20(cont.). Backscattering coefficient of Gaussian surface, $\sigma=0.7163$ units, horizontal polarization.

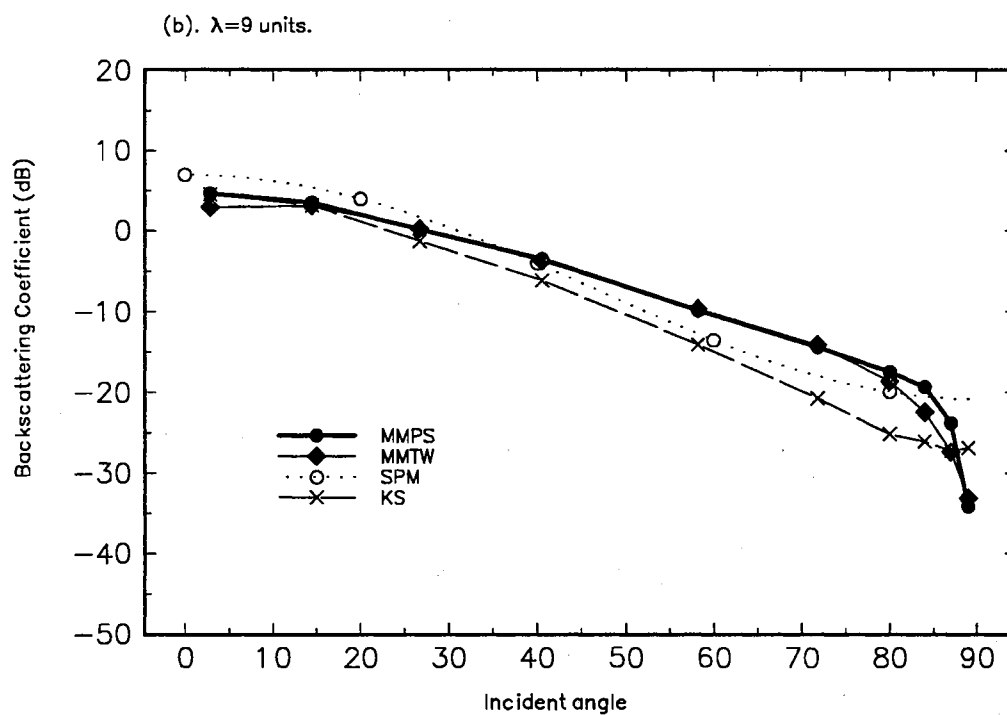
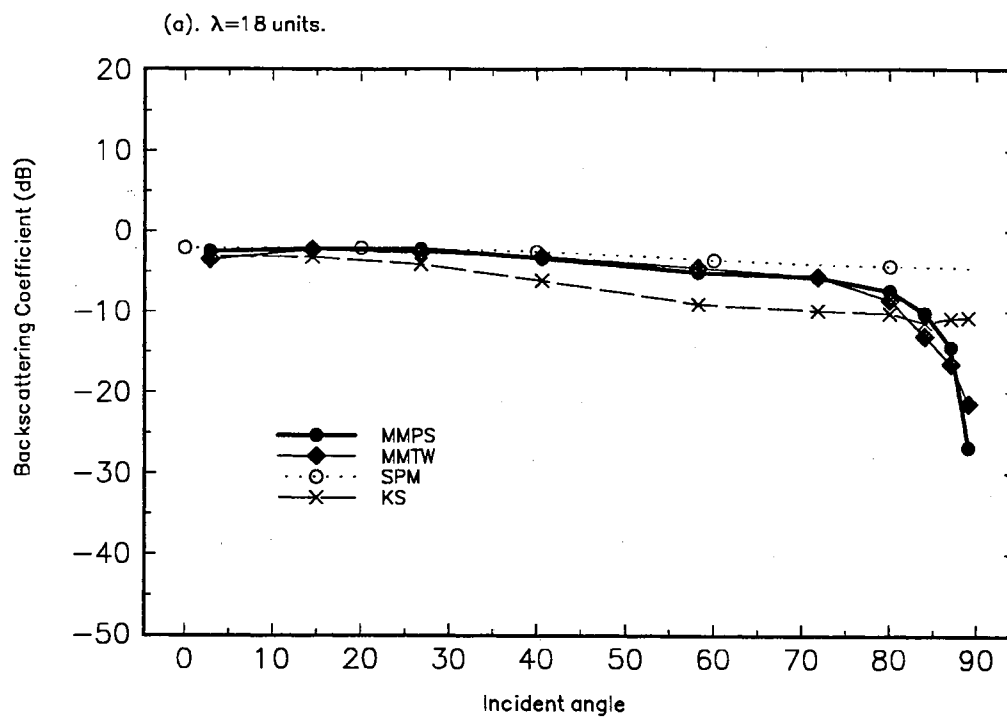


Figure 21. Backscattering coefficient of Gaussian surface, $\sigma=0.7163$ units, vertical polarization.

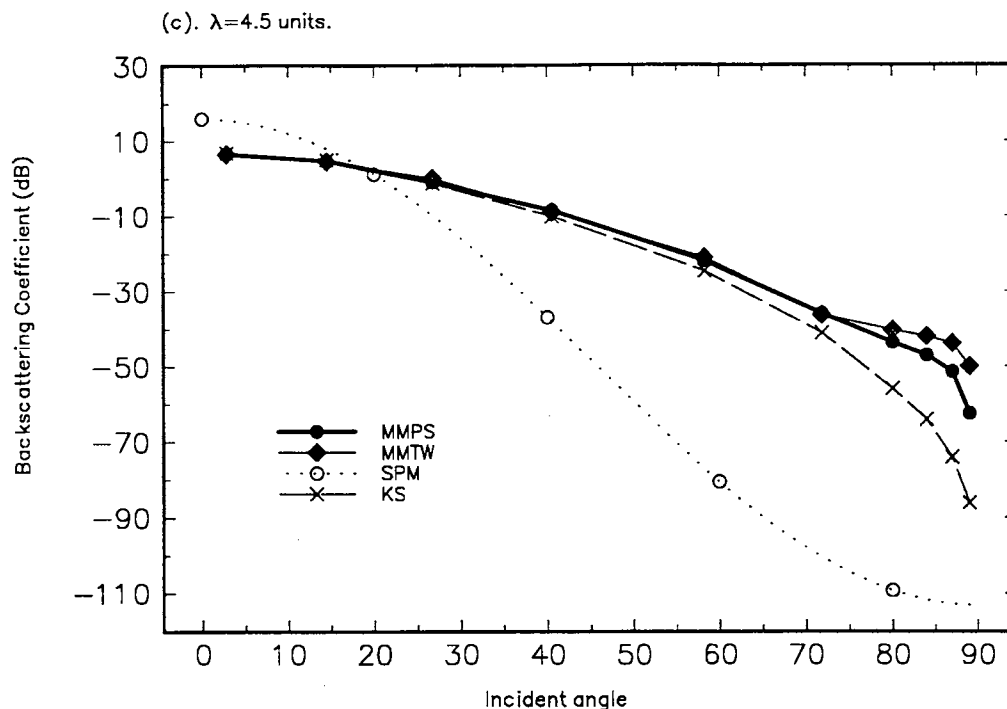


Figure 21(cont.). Backscattering coefficient of Gaussian surface, $\sigma=0.7163$ units, vertical polarization.

met. This study shows that these conditions are also sufficient at horizontal polarization at incident angles up to 89° . At vertical polarization, SPM is valid under these conditions at incident angles up to 70° . At higher angles, the actual scattering drops rapidly while SPM predictions remain approximately constant. Possible reasons for this discrepancy are the excitation of surface waves and diffraction that SPM does not predict, and are not present at horizontal polarization.

The Kirchhoff approximation has previously been shown to be valid when the locally projected radius of curvature is large comparable to or larger than the wavelength, (equation (6-6) and (6-7)). These calculations show that these conditions are sufficient at angles of incidence up to 85° at horizontal polarization and up to 70° at vertical polarization. The discrepancies at higher incidence angles are due to the self-shadowing introduced by the very rough surface and (at vertical polarization) wave diffraction.

Scattering from Power-Law Surfaces

Natural surfaces are much better described by power-spectral densities that follow an inverse power law (Kim, 1992). Here we examine scattering from surfaces whose power-spectral-density is given by

$$W(K) = \begin{cases} 0 & |K| < K_0 \\ \frac{\alpha}{8|K|^3} & |K| \geq K_0 \end{cases} \quad (6-20)$$

where α is a dimensionless constant equal to 8.1×10^{-3} and K_0 is an arbitrary wave number threshold that will be varied in the scattering calculations. This spectrum corresponds to the saturated region of the one-dimensional Pierson-Moskowitz ocean wind-wave spectrum (Thorsos, 1990). The variance of the surface height is

$$\sigma^2 = \int_{-\infty}^{\infty} dK W(K) = \frac{\alpha}{4K_0^2} \quad (6-21)$$

Figure 22(a) shows a typical surface whose roughness spectrum is given by (6-20). Note that this surface has significantly greater high-frequency energy than the Gaussian surface of Figure 17(a). Figure 22(b) shows the autocorrelation estimated from 100 sample surfaces generated using the spectral technique. Also shown is the theoretical autocorrelation, obtained by numerically integrating the inverse Fourier transform of equation (6-20). The calculated and theoretical autocorrelations show excellent agreement. Compared with Gaussian surface in the previous section we should note that power-law surface is multiscale surface and much rougher than Gaussian surface when both surfaces have the same correlation length.

The statistics of the power-law surface are defined entirely by the standard deviation σ . Given σ , the wave number threshold K_0 is determined from equation (6-21). Moreover, with a fixed α the K^{-3} dependence of the spectrum ensures that the radar scattering is a

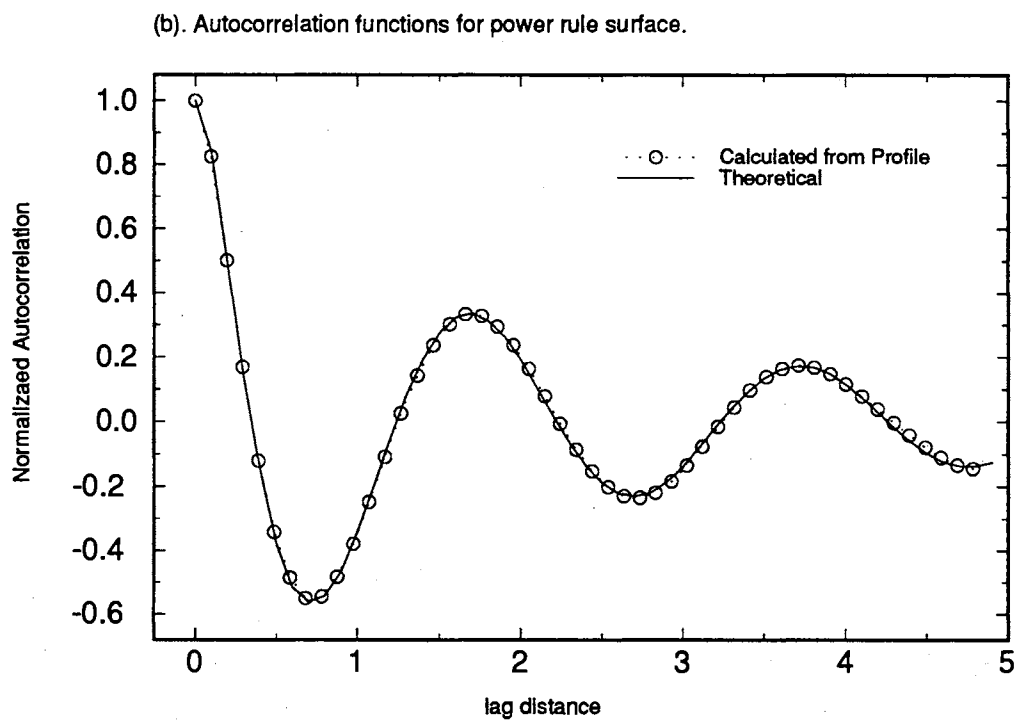
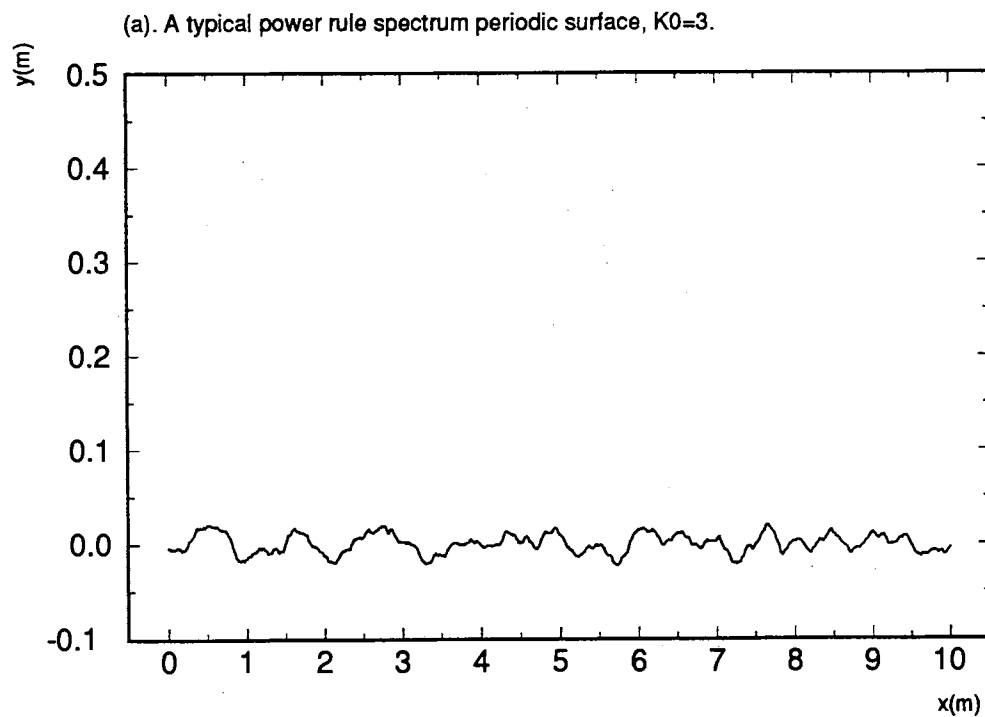


Figure 22. A typical power-law spectrum periodic surface and its autocorrelation function. $K_0=3$.

function of the standard deviation normalized to the radar wavelength (σ/λ) (Rodriquez et al., 1992). Therefore, the scattering from power-law surfaces with three different σ/λ values was calculated. The surface parameters used are summarized in Table 2. $\Lambda_0 = 2\pi/K_0$ is the longest surface wavelength included in the surface spectrum.

Table 2. Parameters used in power-law surface scattering calculations.

| K_0/k | σ/λ | Λ_0/λ |
|---------|------------------|---------------------|
| 0.00716 | 1 | 140 |
| 0.0716 | 0.1 | 14 |
| 0.716 | 0.01 | 1.4 |

The sample surface from which the scattering is calculated should contain at least one cycle of the lowest non-zero wave number in the spectrum. Thus, the surface length must meet

$$L > \frac{2\pi}{K_0} \quad (6-22)$$

Table 3 summarizes the numerically modeled surface lengths at the various surface roughnesses and angles of incidence. Note that when $L=139\lambda$ the moment method sampling period was increased to $\lambda/7$ to avoid excessive computational time. Thus, this case will produce slightly less accurate results than the other cases where $\lambda/10$ was used.

Table 3. Surface lengths used in PS model computations.

(a). $\sigma/\lambda = 0.01$, $K_0/k=0.00716$.

| | | | | | | | | | | | |
|-------------------|------|------|-------|-------|------|-------|-------|-------|-----|------|------|
| θ (degree) | 2.86 | 8.63 | 14.48 | 20.49 | 21 | 33.37 | 48.59 | 71.81 | 82 | 87 | 89 |
| $L(\lambda)$ | 10 | 10 | 10 | 10 | 9.73 | 10 | 10 | 10 | 9.6 | 9.53 | 9.53 |

(b). $\sigma/\lambda = 0.1$, $K_0/k=0.0716$.

| | | | | | | | | | | | |
|-------------------|-------|------|-------|-------|-------|------|-------|-------|-------|-------|-------|
| θ (degree) | 2 | 2.15 | 13.74 | 29.18 | 43.43 | 59.6 | 69.64 | 80.93 | 84 | 87 | 89 |
| $L(\lambda)$ | 42.98 | 40 | 40 | 40 | 40 | 40 | 40 | 40 | 39.72 | 39.55 | 39.51 |

(c). $\sigma/\lambda = 1$, $K_0/k=0.716$

| θ (degree) | 1.43 | 7.18 | 18.96 | 31.67 | 46.47 | 61.05 | 77.16 | 84.27 | 89 |
|-------------------|--------|--------|--------|--------|--------|--------|--------|--------|--------|
| $L(\lambda)$ | 139.63 | 139.63 | 139.63 | 139.63 | 139.63 | 139.63 | 139.63 | 139.63 | 139.62 |

Results

Figure 23 shows the scattering coefficients calculated for the power-law surfaces at horizontal polarization. Also shown are the theoretical scattering coefficients calculated using the small-perturbation model and the Kirchhoff approximation. The surface roughness in part (a) of the figure was $\sigma/\lambda=0.01$. There is a dramatic change in the backscatter at $\theta_i=20^\circ$. At this angle, the Bragg resonance condition is met for the lowest

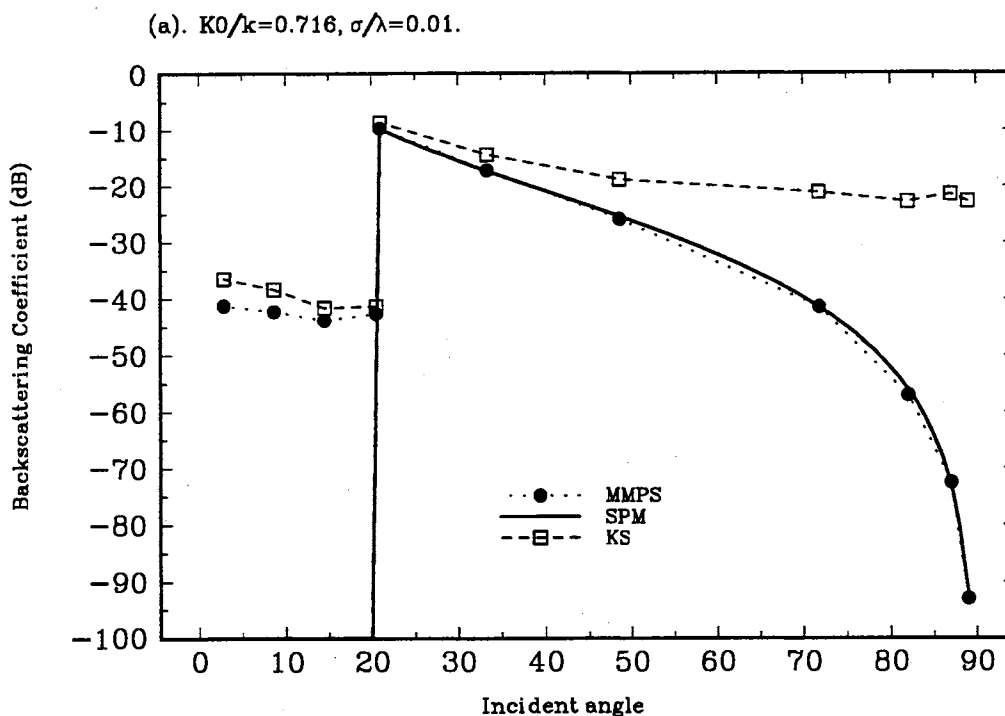


Figure 23. Backscattering coefficient of power-law surface (K^{-3}) at horizontal polarization.

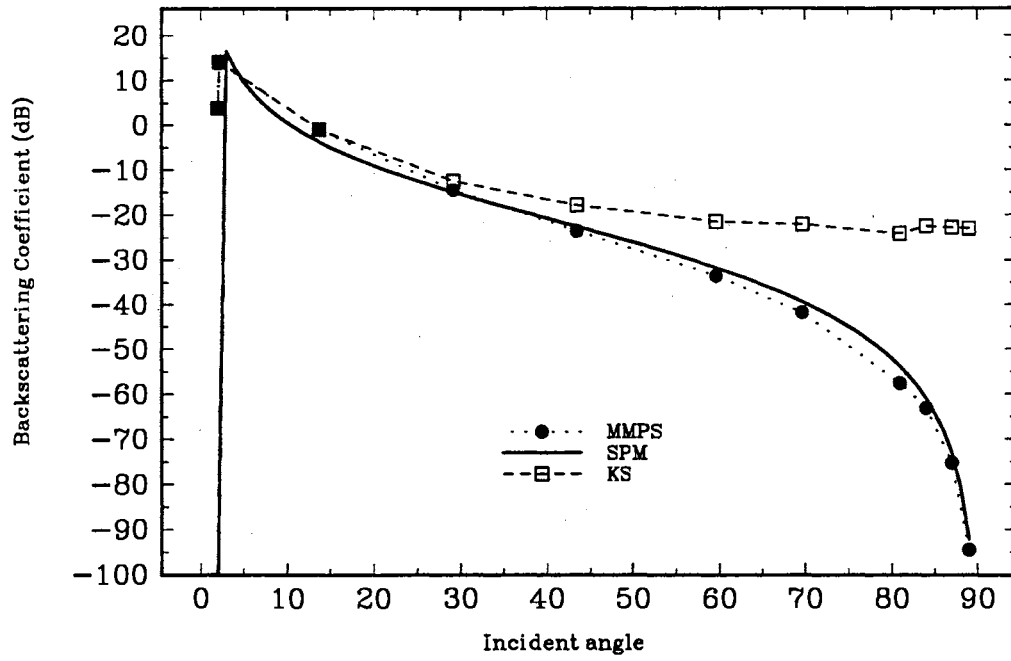
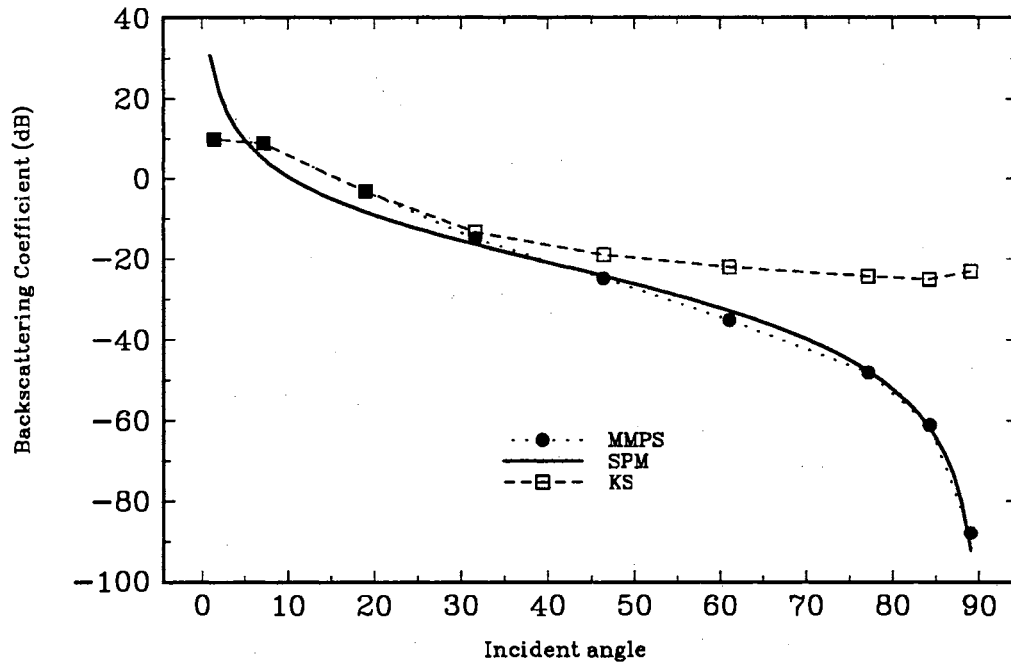
(b). $K0/k=0.0716$, $\sigma/\lambda=0.1$.(c). $K0/k=0.00716$, $\sigma/\lambda=1$.

Figure 23(cont.). Backscattering coefficient of power-law surface (K^{-3}) at horizontal polarization.

wave number included in the surface spectrum:

$$K_0 = 2k \sin \theta_i \quad (6-23)$$

At angles of incidence below 20° , there are no surface wave components that are first order Bragg-resonant, so SPM predicts no backscatter. The Kirchhoff approximation shows fair agreement with the numerical results in this region. At all incident angles above 20° , SPM agrees with the numerical results to within 1dB.

Figure 23(b) is the backscattering coefficients when the surface roughness was increased to $\frac{\sigma}{\lambda}=0.1$. Because the threshold K_0 is smaller for this surface, the angle below which SPM predicts no backscatter is much smaller. At angles of incidence greater than 20° , SPM and the numerical calculations show excellent agreement. At lower angles, the Kirchhoff approximation gives a better prediction of the calculated scattering (to within 1dB).

Figure 23(c) shows the backscattering coefficients calculated for a very rough surface ($\sigma/\lambda = 1$). SPM predictions agree with the numerical calculations to within 3 dB at angles of incidence greater than 30° . At smaller angles, the Kirchhoff approximation gives a very accurate prediction of the numerical calculations, but again diverges rapidly at higher angles.

Figure 24 repeats the calculations in Figure 23 at vertical polarization. The surface roughness was $\sigma/\lambda=0.01$ in part (a). Again, the calculated scattering changed dramatically at the incident angle given by equation (6-23). Above this threshold, SPM shows excellent agreement with the numerical calculations at all but the largest incidence angles. When $\theta_i > 88^\circ$, the numerical values drop rapidly while the SPM results remain about constant. The Kirchhoff approximation is accurate at about $\theta_i=30^\circ$, but diverges at higher and lower angles.

Figure 24(b) shows the results when the surface roughness was $\sigma/\lambda = 0.1$. SPM agrees with the numerical calculations at angles of incidence ranging from about 25° to 85° . At higher angles the numerical results drop rapidly while SPM remains approximately constant. Below 25° , the Kirchhoff approximation yields a very good prediction of the numerical scattering.

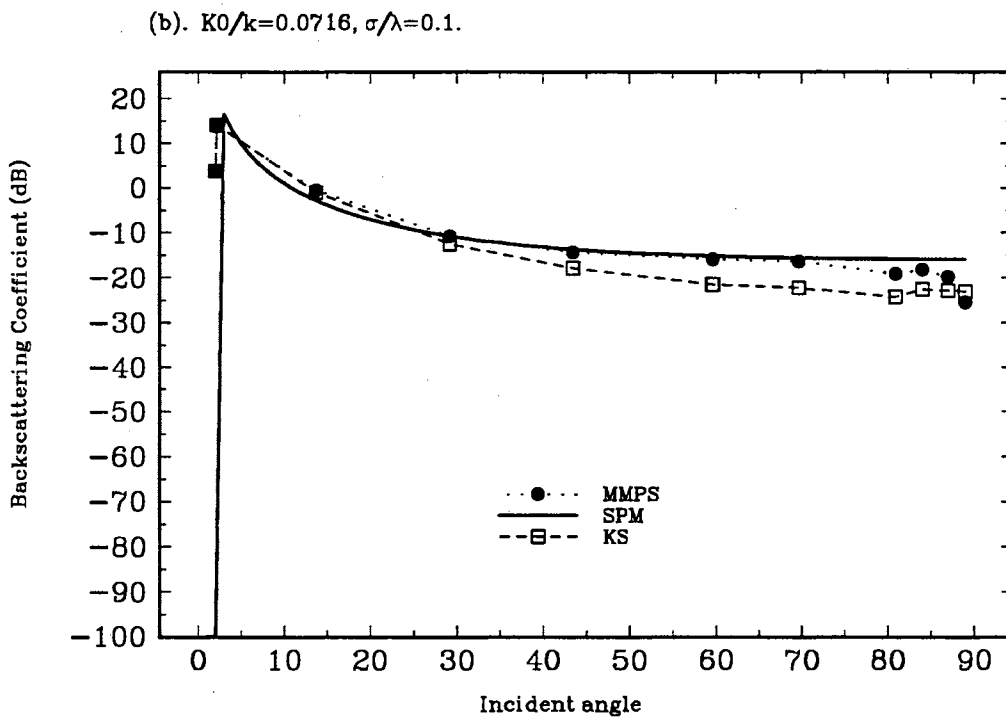
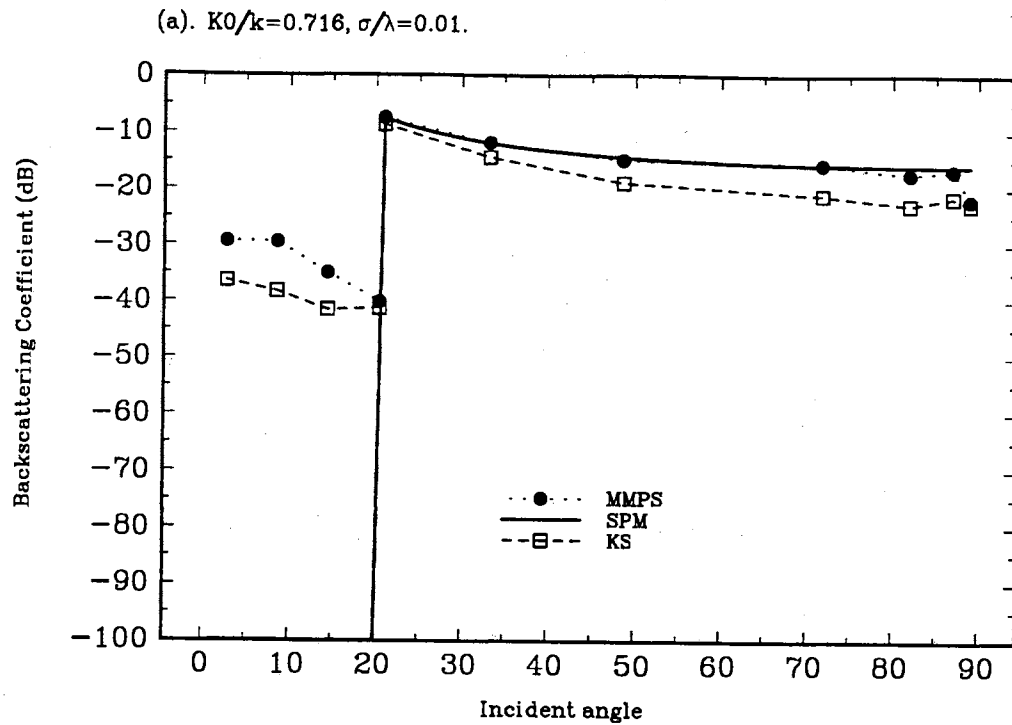


Figure 24. Backscattering coefficient of power-law surface (K^3) at vertical polarization.

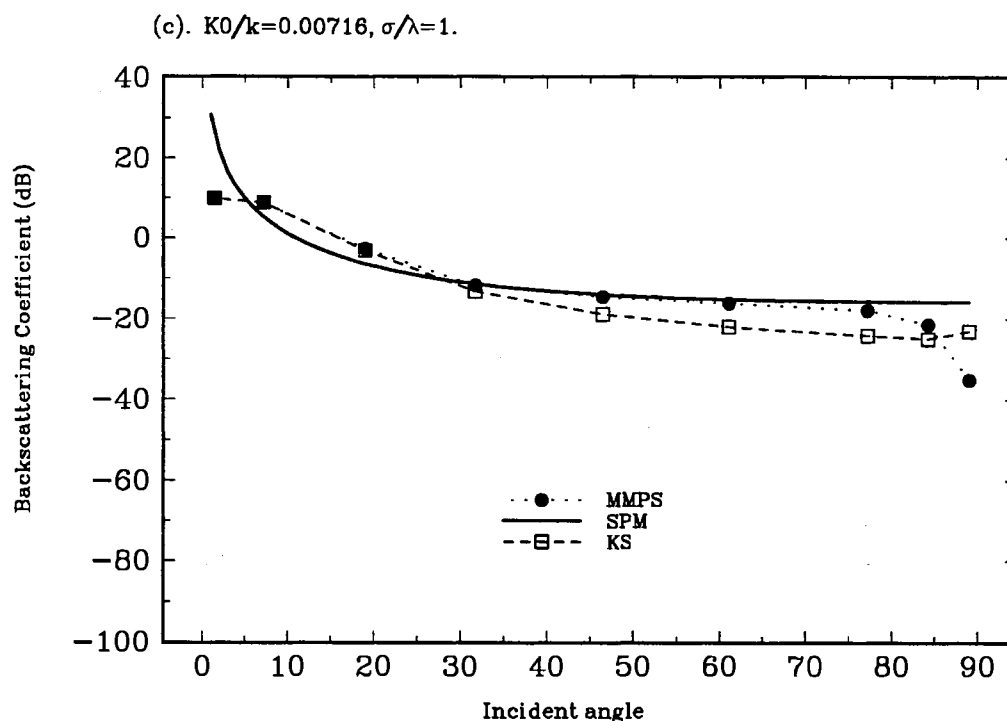


Figure 24(cont.). Backscattering coefficient of power-law surface (K^{-3}) at vertical polarization.

Figure 24(c) shows the calculated backscattering coefficient from the very rough surface where $\sigma/\lambda=1.0$. In this case, the range of validity of SPM has reduced to $30^\circ < \theta_i < 80^\circ$. The Kirchhoff model again shows excellent agreement with the numerical calculations at smaller incidence angles.

Discussions

When $\sigma/\lambda=0.01$ or $\sigma/\lambda=0.1$, the conditions for the validity of SPM are met. Therefore, it is not surprising that the SPM theoretical results agree well with the numerical calculations at angles of incidence above 20° (the minimum where SPM is valid for any surface) for these surfaces except very large angles at vertical polarization (where SPM was shown to be invalid in the study of Gaussian surface scattering). When $\sigma/\lambda=1.0$ (Figures 23(c) and 24(c)), the condition $k\sigma = 2\pi\sigma/\lambda < 0.3$ is not met. However, SPM still

gives an accurate prediction of the scattering for this surface at moderate and large angles (again except for the largest angles at vertical polarization) while the Kirchhoff approximation gives good results at smaller angles. This can be understood using a two-scale description of the surface (Wright, 1968). In this, a threshold is artificially introduced into the surface spectrum. The surface displacement introduced by surface-wave energy above the threshold is small compared to the radar wavelength, and SPM is used to predict the backscattering from this small-scale roughness at moderate and large angles of incidence. The surface-wave energy at wave numbers below the scale transition gives displacements that are large compared to the radar wavelength. This wave energy contributes to the backscatter in two ways. At small incidence angles, this large-scale roughness meets the criterion for the Kirchhoff approximation to be valid, and the electromagnetic energy is scattered through this mechanism. At moderate and large incidence angles, the large-scale roughness changes the local incidence angle and therefore the Bragg resonance condition. However, since the large-scale tilt is random, its effects are averaged out when the scattering from large areas is calculated. The scattering characteristics exhibited in Figures 23(c) and 24(c) closely follow that expected for a two-scale surface, thereby showing that the two-scale model accurately predicts the scattering from the power-law surface at all angles of incidence and both polarization, except for vertical polarization at extremely large incidence angles.

The results here further suggest that the reduction in backscatter at vertical polarization at extremely large angles of incidence is due to surface shadowing and diffraction effects. When $\sigma/\lambda=0.01$, the surface roughness is quite small, and parts of the surface will be shadowed only when the incident angle is extremely large, corresponding to the reduction in scattering at only the largest incidence angles in Figure 24(a). As σ/λ increases, surface shadowing will occur at smaller angles, thereby giving the reductions at smaller angles exhibited by Figures 24(b) and 24(c). As was the case with Gaussian surfaces, scattering at horizontal polarization appears to be much less susceptible to this effect.

CHAPTER VII

SUMMARY AND CONCLUSIONS

The moment method has been investigated as a technique to numerically predict the scattering of electromagnetic waves from a rough surface such as the ocean surface at large angles of incidence (small grazing angles). Use of an illumination weighting function had been shown to give incorrect results at this angular region. Instead, an approach that assumes the surface is periodic was adopted. Using this assumption introduces an infinite summation into the integral equations that describe the scattering. Numerically truncating the summation to a finite number of periods introduces an edge diffraction component into the calculated scattered field (edge effects). The edge effects are strongly dependent on the incident angle and physical size of surface included in the summation (the period of the surface multiplied by the number of periods). At very large incident angles (small grazing angles) many terms must be included in the summation, so direct evaluation of all moment matrix elements is cost prohibitive.

A technique to efficiently evaluate the summations has been developed. It expands the summation into a series of universal summations that are identical for every matrix element, plus a much smaller direct summation that includes the dependence on the individual elements. Use of these universal summations requires only a slight increase in computation time over traditional methods that use only a single period, but yields much greater accuracy at large incident angles. The model has been developed for horizontal and vertical polarization scattering using both electric field and magnetic field integral equation moment method implementations.

The accuracy of the model has been investigated through theoretical analysis and application to practical scattering problems. At small incident angles, discretization errors due to the moment method sampling of the surface dominate. At large incident angles

the errors introduced by edge diffraction (edge effects) dominate. This error can be reduced by increasing the number of periods included in the surface or by increasing the period itself, thereby physically moving the edge farther from the reference section. By including enough sections, the model can be applied even at very small grazing angles.

The models were applied to slightly-rough simple surfaces whose theoretical scattering characteristics are well known. Bragg resonant scattering was accurately predicted, and the edge effects at small grazing angles were reduced to well below the scattering coefficients expected for actual surfaces. Similar results were obtained using the EFIE or MFIE formulations for horizontal polarization and the MFIE formulation for vertical polarization, although the EFIE model achieved acceptable results with somewhat fewer periodic sections than the MFIE model at horizontal polarization. It was shown that 100,000 surface periods must be included in the universal summations to reduce the edge-effect scattering to levels well below the expected rough-surface scattering at angles of incidence up to 89° .

The models were also applied to random rough surfaces. The calculated scattering coefficients were compared to the predictions of the small perturbation method and Kirchhoff approximate scattering theories, and to the scattering calculated using the traditional moment method using an illumination weighting function. Analysis of the scattering from surfaces whose power spectral densities are described by Gaussian envelopes confirmed that the periodic surface moment method can be used at incident angles up to 89° at both horizontal and vertical polarization. SPM gives a very good prediction of the scattering from small-scale rough (with respect to radar wavelength) surfaces at all incident angles at horizontal polarization. At vertical polarization, SPM fails to predict the rapid drop in scattering at large incident angles that appears in the numerical results. The Kirchhoff approximation accurately models the scattering from large-scale rough surfaces at large incident angles at horizontal polarization, but significantly under predicts the scattering at vertical polarization.

The scattering from a power-law spectrum surface was also examined. The relative roughness of the surface was varied by changing the threshold K_0 of the minimum wavenumber that was included in the surface spectrum. When the surface roughness is small compared to the radar wavelength, SPM agrees well with numerical calculations at

horizontal polarization at all incident angles where a Bragg resonant surface wave is present, including near-grazing angles. At vertical polarization, SPM again fails to predict the rapid decrease in scattering at large incidence angles. The magnitude of this reduction depends on the surface roughness, indicating that it is at least partially due to surface shadowing. When the rms roughness of the power-law surface is large compared to the radar wavelength, the scattering characteristics are similar to that predicted by the two-scale surface scattering model at both polarizations, at low incident angles the Kirchhoff approximation is valid, while at large incident angles SPM applies. The primary discrepancy is that again the scattering drops rapidly at large incidence angles at vertical polarization, a characteristic that is not predicted by SPM.

REFERENCES

- Andreasen, M. G. (1964). Scattering from parallel metallic with arbitrary cross sections, IEEE Trans. Ant. Prop., 12(6), 746-754.
- Axline, R. M., & Fung, A. K. (1978). Numerical computation of scattering from a perfectly conducting random surface, IEEE Trans. Antennas Propag., 26, 482-488.
- Broschat, S. L. (1993). The phase perturbation approximation for rough surface scattering from a Pierson-Moskowitz sea surface. IEEE Trans. on Geoscience and Remote Sensing, 31(1), 278-283.
- Bahar, E. (1981). Scattering cross sections for composite random surfaces: Full wave analysis, Radio Sci., 16(6), 1327-1335.
- Balanis, C. A. (1989). Advanced engineering electromagnetics, John Wiley & Sons Inc.
- Beckmann, P., & Spizzichino, A. (1963). The Scattering of Electromagnetic Waves From Rough Surfaces, Macmillan, New York .
- Boag, A., & Leviatan Y. (1989). Analysis of two-dimensional electromagnetic scattering from nonplanar periodic surfaces using a strip current model, IEEE Trans. AP 37, 1437-1445.
- Brown, G. S. (1978). Backscattering from a Gaussian-distributed, perfectly conducting rough surface, IEEE Trans. Antennas Propag., 26, 472-482.
- Burke, G. J., & Poggio A. J. (1977). Numerical electromagnetic code (NEC)-Method of moments, Naval Ocean Systems Command Technical Document 116.
- Chan, H. L., & Fung, A. K. (1978). A numerical study of the Kirchhoff approximation in horizontally polarized backscattering from a random surface. Radio Sci., 13, 811-818.
- Chen, M. F., Chen, D. S., & Fung, A. K. (1989). A study of the validity of the integral equation model by moment method simulation -- cylindrical case, Remote Sens. Environ. 29, 217-228.

- Chen, M. F., & Fung, A. K. (1988), A numerical study of the regions of validity of the Kirchhoff and small-perturbation rough surface scattering modes, Radio Sci., 23, 163-170.
- Chen, R. (1990). Moment method for scattering from 2-D arbitrary conducting cylinder, ECEN 6050 report, Oklahoma State University.
- Durden, Stephen L., & Vesecky, J. F. (1990). A numerical study of the separation wave number in the two-scale scattering approximation. IEEE Trans. on Geosci. and Rem. Sens. 28(2), 271-272.
- Fung, A. K., & Chen, M. F. (1985). Numerical simulation of scattering from simple and composite random surfaces, J. Opt. Soc. Am. A, 2, 2274-2284.
- Glisson, A. W., & Wilton, D. (1980). Simple and efficient numerical methods for problems of electromagnetic radiation and scattering from surfaces, IEEE Trans. Ant. Prop., 28(5), 593-603.
- Green, O. B. (1970). Diffraction efficiencies for infinite perfectly conducting gratings of arbitrary profile, IEEE Trans. Microwave Theory and Techniques, 18(6), 313-318.
- Guinard, N. W. (1970). An experimental study of a sea clutter model, Proceedings of the IEEE, 58(4), 543-550.
- Harrington, R. (1967). Matrix methods for fields problems, Proc. IEEE, 55, 136-149.
- Harrington, R. (1968). Field computation by method of moments, Macmillan, New York.
- Herrmann, G. F. (1990). Note on interpolational basis functions in the method of moments, IEEE Trans. Ant. Prop., 38, 134-137.
- Hessel, A., & Oliver, A. A. (1965). A new theory of wood's anomalies on optical grating, Appl. Opt., 4, 1275-1297.
- Ingber, M. S., & Ott, R. H. (1991). An application of the boundary element method to the magnetic field integral equation, IEEE Trans. Ant. Prop., 39 (5), 606-611.
- Jordan, A. K., & Lang, R. H., (1979). Electromagnetic scattering patterns from sinusoidal surfaces, Radio Sci., 14(6), 1077-1088.
- Kalhor, H. A. (1989). Plane metallic Gratings of finite numbers of strips, IEEE Trans. Ant. Prop., 37, 406-407.

- Kim, Y., Rodriguez, E., & Durden, S. L. (1992). A numerical assessment of rough surface scattering theories: vertical polarization, Radio Sci. 27(4), 515-527.
- Kim, Y., Rodriguez, E., & Lou S.-H. (1992). Numerical evaluation of rough surface scattering at near grazing incidence. URSI Radio Science Meeting, Chicago, USA, 399.
- Kress, R. (1990). Numerical solution of boundary integral equations in time-harmonic electromagnetic scattering, Electromagn. 10, 1-20.
- Lentz, R. R. (1974). A numerical study of electromagnetic scattering from ocean-like surfaces, Radio Sci., 9(12), 1139-1146.
- Lou, S. H., Tsang, L., Chan, C. H., & Ishimaru, A. (1990). Monte Carlo simulations of scattering of waves by a random rough surface with the finite element method and the finite difference method, Microwave and Optical Technology Letters, 3(5), 150-154.
- Lou, S. H., Tsang, L., Chan, C. H., & Ishimaru, A. (1991). Application of the finite element method to Monte Carlo simulations of scattering of waves by random rough surfaces with the periodic boundary condition, Journal of Electromagnetic Waves and Applications, 5(8), 835-855.
- McDaniel, S. T., & Gorman, A. D. (1983). An examination of the composite-roughness scattering model, J. Acoust. Soc. Am., 73, 1476-1486.
- Mitra, R. (1973). Computer techniques for electromagnetics. New York: Pergamon.
- Morgan, M. A. (ed.), (1990). Finite element and finite difference methods in electromagnetic scattering, Progress in Electromagnetic Research, 2, Elsevier, New York.
- Ney, M. M. (1985). Method of moments as applied to electromagnetic problems, IEEE Microwave Theory and Tech., 33(10), 972-980.
- Nieto, V. M., & Garcia, N. (1981). A detailed study of the scattering of scalar waves from random rough surfaces, Opt. Acta, 28(12), 1651-1672.
- Peterson, A. F., & Mitra, R. (1987). Iterative-based computational methods for electromagnetic scattering from individual or periodic structures, IEEE Oceanic Eng., 12, 458-465.

- Rao, S. M., Wilton, D. R., & Glisson, A. W. (1982), Electromagnetic scattering by surfaces of arbitrary shape, IEEE Trans. Ant. Prop., 30(5), 409-418.
- Rodriguez, E. (1989). Beyond the Kirchhoff approximation, Radio Sci., 24, 681-693.
- Rodriguez, E., Ernesto, K., J., & Durden, S. L. (1992). A numerical assessment of rough surface scattering theories: Horizontal polarization, Radio Sci., 27(4), 497-513.
- Sarkar, T. K., & Mittra, R. (1985). An iterative moment method for analyzing the electromagnetic field distribution inside inhomogeneous lossy dielectric objects, IEEE Trans. Microwave Theory Tech., 33, 163-167.
- Sarkar, T. K., Siarkiewicz, K. R., & Stratton, R. F. (1981). Survey of numerical methods for solutions of large systems of linear equations for electromagnetic field problems, IEEE Trans. Antennas Propagat., 29, 847-856.
- Silvester, P. P. (1969). High-order polynomial triangular finite elements for potential problems, Int. J. Engng. Sci. 7, 849-861.
- Sklar, B. (1988). Digital Communications, Fundamentals and Applications, Prentice Hall, Englewood Cliffs, New Jersey.
- Rice, S. O. (1951). Reflection of electromagnetic waves from slightly rough surfaces, Commun. Pure Appl. Math., 4, 351-378.
- Shen, J., & Maradudin A. A. (1980). Multiple scattering of waves from random rough surfaces, Phys. Rev., 22(9), 4234-4240.
- Thorsos, E. I. (1988). The validity of the Kirchhoff approximation for rough surface scattering using a Gaussian roughness spectrum, J. Acoust. Soc. Am., 83(1), 78-82.
- Thorsos, E. I., & Jackson, D. R. (1989). The validity of the perturbation approximation for rough surface scattering using a Gaussian roughness spectrum, J. Acoust. Soc. Am., 86(1), 261-277.
- Thorsos, E. I. (1990). Acoustic scattering from a 'Pierson-Moskowitz' sea surface, J. Acoust. Soc. Am., 88, 335-349.
- Twersky, V. (1956), On the scattering of waves by an infinite grating, IRE Trans. Ant. Prop., 4, 330-345.
- Truang, S. L., Shah, V. & Tamir, T. (1981). Scattering of waves from periodic surfaces, Proc. IEEE, 69, 1132-1144.

- Ulaby, F. T., Moore, R. K., & Fung, A. K. (1982). Microwave remote sensing, Vol. II, Artech House, INC.
- Wetzel, L. B. (1977). A model for sea backscatter intermittency at extreme grazing angles, Radio Sci, 12, 749,756.
- Winebrenner, K. P., & Ishimaru, A. (1985a). Investigation of a surface field phase perturbation technique for scattering from rough surfaces, Radio Sci., 20, 161-170 .
- Winebrenner, K. P., & Ishimaru, A. (1985b). Application of the phase perturbation technique to randomly rough surfaces, J. Opt. Soc. Am. A, 2, 2285-2293.
- Zaki, K. A. & Neureuther, A. R. (1971), Scattering from a perfectly conducting surface with a sinusoidal height profile: TE polarization, IEEE Trans. Ant. Prop., 19, 208-214.

VITA 2

Ruimin Chen

Candidate for the Degree of

Doctor of Philosophy

Thesis: NUMERICAL INVESTIGATION OF ELECTROMAGNETIC SCATTERING
FROM THE OCEAN SURFACE AT EXTREME GRAZING ANGLES

Major Field: Electrical Engineering

Biographical:

Personal Data: Born in Yinnan, the People's Republic of China, April 12, 1957, the son of XiLan Duan and Deshen Chen.

Education: Graduated from the 55th High School, Chongqing, China, in July 1975; received Bachelor of Science Degree in July, 1982 and Master of Science Degree in May, 1985, in Electrical Engineering from Chongqing University, Chongqing, China, respectively; completed requirements for the Degree of Doctor of Philosophy at Oklahoma State University in May, 1994.

Professional Experience: Teaching and Research Lecturer, Department of Radio Communication Engineering, Nanjing Institute of Communication Engineering, China, August, 1985, to May 1990; Teaching and Research Assistant, Department of Electrical and Computer Engineering, Oklahoma State University, June 1990, to December, 1993.

Name: Ruimin Chen

Date of Degree: May, 1994

Institution: Oklahoma State University

Location: Stillwater, Oklahoma

Title of Study: NUMERICAL INVESTIGATION OF ELECTROMAGNETIC
SCATTERING FROM THE OCEAN SURFACE AT EXTREME
GRAZING ANGLES

Pages in Study: 82

Candidate for the Degree of
Doctor of Philosophy

Major field: Electrical Engineering

Scope and Method of Study: The investigation of radar scattering from the ocean surface at large angles of incidence (small grazing angles) is of interest for scientific and military applications. Many approximate theories exist to describe scattering from the ocean surface, but their validity at small grazing angles is unknown. Traditional numerical techniques for surface scattering calculations cannot be directly applied under these conditions. In this work the moment method is extended to model rough surface scattering at very large angles. The modeled surface is treated as periodic, thereby eliminating nonphysical edge diffraction effects. A set of universal summations that are common to all moment method matrix elements are derived to efficiently evaluate the infinite summations that appear in integral equations describing scattering from periodic surfaces. Computational efforts to apply the technique to model reflection from an infinite flat plate and scattering from simple slightly-rough surfaces confirm that the edge effects, including those at great incident angles, are reduced to acceptable levels.

Findings and Conclusions: The extended moment method has been applied to evaluate the scattering from random rough surfaces whose power spectral densities are defined by both Gaussian and power law functions. The treatment of Gaussian surfaces confirms that the technique can be used to accurately calculate the scattering from random rough surface at incidence angles up to at least 89° . At horizontal polarization, comparison of the numerically calculated scattering with the predictions of existing approximate theories shows that these theories can be applied at large incidence angles under the same surface conditions for which they were already known to be valid at moderate incidence angles. At vertical polarization, the approximate theories fail at extremely large incidence angles. The threshold at which the theories fail depends strongly on the surface roughness characteristics.

ADVISER'S APPROVAL